Modeling Thermal Turbulence Using Implicit Large Eddy Simulation

Master's Thesis

By

Md Naim Hossain

CIMNE
Universitat Politecnica de Catalunya

A thesis submitted for the degree of
Master of Science in Computational Mechanics

Accomplished on
June 2012

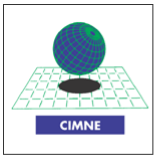

Supervised by

Prof. Ramon Codina
Department of Strength of Materials and Structural Engineering
(RMEE)
and
International Center for Numerical Methods in Engineering
(CIMNE)
Universitat Politecnica de Catalunya
Barcelona, Spain

Dedication

To my parents for their endless love and support

Abstract

A general description of a thermally coupled fluid flow is given by the incompressible Navier-Stokes equations coupled with the heat equation using Boussinesq approximation, whose mathematical structure is much well understood. A variational multiscale finite element approximation has been considered for the formulation of incompressible Navier-Stokes equation and heat equation. The complexity of these problems makes their numerical solution very difficult as the standard finite element method is unstable. In the incompressible Navier Stokes equations, two well known sources of numerical instabilities are the incompressibility constraint and the presence of the convective term. Many stabilization techniques used nowadays are based on scale separation, splitting the unknown into a coarse part induced by the discretization of the domain and a fine subgrid part. The modeling of the subgrid scale and its influence leads to a modified coarse scale problem providing stability.

In convection-diffusion problem once global instabilities have been overcome by a stabilization method, there are still local oscillations near layers due to the lack of monotonicity of the method. Shock capturing techniques are often employed to deal with them. Proper choice of stabilization and shock capturing techniques can eliminate the local instabilities near layers of convection-diffusion equation.

A very important issue of the formulation presented in this thermally coupled incompressible flow is the possibility to model turbulent flows. Some terms involving the velocity subgrid scale arise from the convective term in the Navier-Stokes equations which can be understood as the contribution from the Reynolds tensor of a LES approach and the contribution from the cross stress tensor. This opens the door of modeling thermal turbulence using LES automatically inherited by the formulation used in this work.

Different classical benchmark problems are numerically solved in this thesis work for the convection-diffusion equation to show the capabilities of different combination of stabilization and shock capturing methods. In the case of thermally coupled incompressible flows some numerical and industrial examples are exhibited to check the performance of the different combination of stabilization and shock capturing methods and to compare them. The objective is to conclude which method works better to approximate the exact solution and eliminate instabilities and local oscillations.

Acknowledgement

I would like to acknowledge my thesis supervisor, Prof. Ramon Codina, whose expertise, patience and insightful guidance helped me a lot during the entire time of my thesis work.

Additionally, I would like to special thank for the constant help, opportune advice and continuous support provided by Joan Baiges.

In addition, a very special thanks to Christian Muñoz, Matias Avila and Héctor G. Espinoza Román from Prof. Ramon Codina's group for their constant help and support facilitated my thesis work.

I would also like to stress the help of my family and friends, from the distance or in person, were very supportive right from the start of this project.

Finally, I would like to express my gratitude to all the people that compose the Erasmus Mundus programme in Computational Mechanics which where always helpful and supportive. Special thanks to Lelia Zielonka for her help since the start of the master course.

Md Naim Hossain
Barcelona, Spain.

Contents

Nomenclature

Latin Symbols

u	Velocity field
p	Pressure field
g	Gravity acceleration vector
f	External Body force
Q	Heat Source
L	Characteristic Length
U	Characteristic Velocity
Ra	Rayleigh Number
Re	Reynolds Number
Pr	Prandl Number
Pe	Peclet Number
C	Courant Number
$\bar{u}$	Large scale of the variable
$\acute{u}$	Small scale of the variable
s	Reaction coefficient
V_h	Finite Element space
$\tilde{V}$	Subgrid space
S	Strain tensor
k	Turbulent kinetic energy and diffusion coefficient
G	Filtering Kernel
P	Production term

Greek Symbols

ϵ	Turbulent Dissipation
μ_t	Turbulent viscosity or Eddy viscosity
τ	Stabilization parameter
ω	Specific dissipation
ν	Kinematic viscosity
α	Thermal expansion coefficient
ϑ	Temperature field

Γ	Boundary
κ	Thermal Diffusivity
θ	Weighting parameter for temporal derivatives
δ	Kronecker delta
Δx	Mesh size or Spatial step
Ω	Computational domain
$\partial\Omega$	Boundary of the computational domain
ϕ	Shape function
Δ	Laplacian
ρ	Density
Φ	Pressure-strain correlation term

Subscripts

h	Associated with approximation solution
i, j, k	Associated with node index number
N	Associated with Neumann boundary
$stab$	Stabilized bilinear form
inv	Inverse inequality
dc	Discontinuity capturing
art	Artificial Diffusion
$\|$	Parallel to streamline
t	First derivatives with respect to t
$\max$	Associated with maximum value
Ω	Associated with inside domain (also d)
$\partial\Omega$	Associated with boundary of the domain (also b)
∞	L_∞ norm
nl	Nonlinear

Superscripts

$\tilde{u}$	Sub scale of the variable
p	Power of integrable
h	Associated with approximation solution
$\perp$	Orthogonal to finite element space
d	Associated with Euclidean norm
ap	approximated subscale

Abbreviations and Acronyms

CFL	Courant-Friedrichs-Lewy Condition

FDM	Finite Difference Methods
FEM	Finite Element Methods
$ASGS$	Algebraic Sub-grid Stabilization
OSS	Orthogonal Sub-scale
$PDEs$	Partial Differential Equations
DS	Dynamic Sub-scale
QSS	Quasi static sub-scale
CD	Crosswind dissipation
ID	Isotropic dissipation
$CDRE$	Convection-Diffusion-Reaction equation
SC	Shock Capturing
DC	Discontinuity Capturing
DMP	Discrete Maximum Principle
$OPGB$	Orthogonal Projection Gradient Based
SGS	Sub Grid Scale
$RANS$	Reynolds Average Navier Stokes
LES	Large Eddy Simulation
DNS	Direct Numerical Simulation
NS	Navier Stokes
ASM	Algebraic Stress Model
RSM	Reynolds Stress Model

List of Figures

List of Tables

Chapter 1

Introduction

Thermally coupled incompressible flows are of particular interest from the numerical point of view for different reasons. Apart from their obvious practical interest, very often these flows exhibit instabilities and even transition to turbulence in situations simpler than for isothermal flows. The numerical modeling of these instabilities that take place in rather simple cases is an excellent test for numerical formulations.

The basic formulation for isothermal incompressible flows has been described in Codina et.al.2007 [42] and extensively studied. As it is explained there, considering the subscales time dependent and tracking them along the iterative process to deal with the nonlinear terms has several benefits, such as a better performance in time of the final formulation, the conservation of momentum or the possibility to model turbulence. Here we will apply this formulation to thermally coupled flows using the Boussinesq approximation.

In the first place we have the instability due to the dominance of the convective term over the viscous one in the high Reynolds number regime. This instability is also present in the scalar convection diffusion problem which is well understood and described in Codina1998 [14]. A stable and accurate approximation to this problem will be presented in the next chapters, where a new definition of the stabilization parameters has proven to give excellent results.

As a second problem, we have the pressure instability that may appear if the compatibility of the velocity and pressure spaces posed by the inf-sup condition is not satisfied. It is not related to the dominance of a term in the equations but rather to the vectorial structure of the problem. When the Navier Stokes equations are written as a system of second order equations, the pressure appears in the first order term and the diffusion matrix is not positive definite, but only semidefinite.

In this work we present a stabilized finite element formulation based on the subgrid scale approach introduced for the incompressible Navier Stokes equations. The idea is to split the solution of the continuous problem φ into a finite element component φ_h and the difference $\tilde{\varphi} = \varphi - \varphi_h$, called subscale, which cannot be reproduced by the finite element mesh. This splitting corresponds to a decomposition of the continuous space V as a direct sum of the finite element space V_h and a subgrid space $\tilde{V}$ to be defined. The approximation of the problem projected onto $\tilde{V}$ which is driven by the strong residual of the finite element problem, will give an approximated subscale $\tilde{\varphi^{ap}}$ whose effect on the discrete problem for φ_h will be taken into account. Hopefully, this approximation will enhance the stability properties of the discrete problem projected on V_h, allowing the use of equal order velocity-pressure interpolations and the solution of convection dominated problems. This approach is a general framework in which it is possible to design different stabilized formulations depending on the approximation performed for solving the fine scale problem and on the selection of

the space of subscales.

The heat equation is a simple convection-diffusion equation coupled here with incompressible Navier-Stokes Equations. When attempting the numerical solution of the heat equation, the first problem identified is the lack of stability of the Galerkin formulation when the convective term is important, which manifest itself as numerical oscillations that pollute the solution in the whole domain and specially near boundary layers. After understanding this problem as a lack of diffusion in the discrete problem, the first solution was to add numerical dissipation developing upwind techniques in the context of the finite difference method. The inconsistent extra terms implied a loss of accuracy and the situation was fixed with the introduction of the SUPG method in Hughes et al.1979 [24] which was analysed by C.Johnson et al.1984 [6]. This method depends on a parameter called the stabilization parameter and denoted usually by τ. Once these stabilization terms are added the global instabilities are overcome but still local oscillations cannot be eliminated. For eliminating global failure shock capturing diffusion terms are added for complete stabilization.

1.1 Objectives

The main objective of this thesis presentation is to propose a finite element formulation for thermally coupled flows based on the variational multiscale formulation Hughes et al.1998 [49]. Here we consider the incompressible Navier-Stokes equations using the Boussinesq approximation to model thermal coupling. The basic idea is to split the unknowns velocity, pressure and temperature, into their finite element component and a subgrid scale component, hereafter referred to as subscale. The particular approximation used for these subscales defines the numerical model. The main feature of the model we propose is that we consider the subscales time dependent and that we keep their effect in all the terms of the equations to be solved, both the nonlinear convective terms of the momentum and the heat equation and in the coupling term due to the Boussinesq model.

Modeling turbulence is an important objective in this thesis work, where different turbulence features will be described specially Reynolds Average Navier Stokes Equation(RANS), Large Eddy Simulation(LES) and Direct Numerical Simulation(DNS). In particular, the subgrid scale modeling in the case of nonlinear problems is intimately related to the problem of turbulence modeling, specially LES which is an entire subject on its own right.

One of the most important objectives of this work is to develop a subgrid scale stabilized finite element formulation for the kind of problems we are considering. To achieve this goal we follow a natural way, starting from the scalar convection diffusion equation in chapter 3, where a new definition of the stabilization parameters is presented. Then we extend these results to the thermally coupled incompressible flow problem in chapter 4. This extension involves two main aspects, the definition of the stabilization parameters, which is treated in chapter 4, and the extension of the stabilization techniques to transient nonlinear problems and finally we extend these results to thermally coupled flows in chapter 4, where the final discrete formulation is presented.

Another important objective is to discuss the shock capturing techniques in chapter 3. Once global instabilities have been overcome, there are still local oscillations near layers due to the lack of monotonicity of the method. Shock capturing techniques are often employed to deal with them. Here, our point of view is that this lack of monotonicity is inherent to the integral as duality pairing intrinsic to the variational formulation of the problem.

The last objective is to develop a code for several numerical tests to check the performance of stabilization and shock capturing techniques. Not only simple numerical tests in 2D are presented in this thesis presentation but also 3D industrial application of thermally coupled flow problems will be considered, to get the insight of how the different combination of stabilization method and shock capturing techniques work in different numerical examples.

1.2 Chapter Overview

- The thesis documentation consists of several chapters. The problem statement of the simplified models that describes the coupling of incompressible Navier Stokes equations and heat equation with Boussinesq approximation will be proposed in Chapter 2. Some basic turbulence models description specially Reynolds Average Navier Stokes(RANS), Large Eddy Simulation(LES) and Direct Numerical Simulation(DNS), have been introduced in this chapter.

- In Chapter 3 the numerical approximation started from multiscale approach of the convection-diffusion equation using stabilization parameters and different stabilized methods. In this chapter different shock capturing techniques have been proposed to eliminate local instabilities and global failure. We will discuss about formulation of time dependent convection-diffusion-reaction equation along with the energy dissipation very briefly. Some numerical examples and benchmark tests of the convection-diffusion problem will be numerically solved to check the performance of different combination of stabilization and shock capturing methods in this chapter.

- The numerical approximation of thermally coupled incompressible flow will be discussed in Chapter 4, starting with Variational Multiscale Approximation and Temporal discretization with additional description of the developments concerning the modeling of the subgrid scales. Conservation properties of the scheme specially linear momentum and heat will be previewed. The aspects of LES modeling through the formulation of subscales has been discussed briefly in this chapter.

- Chapter 5 presents the results of numerical examples of thermally coupled incompressible flows proposing at first a simple numerical example of a differential heated cavity with aspect ratio 8 by 1. Then simple 2D numerical modeling of hot fluid injection in a storage tank are discussed to check the performance of different combination of the stabilization and shock capturing techniques.

- In Chapter 6 industrial application of thermally coupled incompressible flow will be proposed extending the 2D numerical example of hot fluid injection in a water storage tank in chapter 5. To get the insight of a 3D numerical modeling and performance check of different shock capturing techniques is the main objective of this chapter.

- In Chapter 7 conclusions and further improvement close this thesis presentation.

Chapter 2

Problem statement and turbulence modeling

In this chapter we describe the problem statement of this thesis which is thermal coupling of incompressible Navier Stokes equations and heat equation using Boussinesq approximation. The boundary and initial conditions are presented along with the problem statement. One of the important aspects of this thesis is modeling thermal turbulence. So starting with the basic idea of turbulence classifications of different kind of turbulence modeling will be discussed briefly in this chapter. Here Reynolds Average Navier Stokes(RANS), Large Eddy Simulation(LES) and Direct Numerical Simulation (DNS) turbulence modeling will be discussed with several computational aspects.

2.1 Problem statement

Let $\Omega \subset \mathbb{R}^d$, with $d = 2, 3$ be the computational domain in which the flow takes place during the time interval $[0, T]$, and let Γ be its boundary. The initial and boundary value problem to be considered consists in finding a velocity field $\boldsymbol{u}$, a pressure p and a temperature ϑ such that:

$$\partial_t \boldsymbol{u} + \boldsymbol{u} \cdot \nabla \boldsymbol{u} - \nu \Delta \boldsymbol{u} + \nabla p + \alpha \boldsymbol{g} \vartheta = \boldsymbol{f} + \alpha \boldsymbol{g} \vartheta_0 \quad \text{in } \Omega, \quad t \in (0, T), \tag{2.1}$$

$$\nabla \cdot \boldsymbol{u} = 0 \quad \text{in } \Omega, \quad t \in (0, T), \tag{2.2}$$

$$\partial_t \vartheta + \boldsymbol{u} \cdot \nabla \vartheta - \kappa \Delta \vartheta = Q \quad \text{in } \Omega, \quad t \in (0, T), \tag{2.3}$$

$$\boldsymbol{u} = \boldsymbol{0} \quad \text{on } \Gamma, \quad t \in (0, T), \tag{2.4}$$

$$\boldsymbol{u} = \boldsymbol{u}^0 \quad \text{in } \Omega, \quad t = 0, \tag{2.5}$$

$$\vartheta = 0 \quad \text{on } \Gamma, \quad t \in (0, T), \tag{2.6}$$

$$\vartheta = \vartheta^0 \quad \text{in } \Omega, \quad t = 0 \tag{2.7}$$

In these equations, ν is the kinematic viscosity, κ the thermal diffusivity, α the thermal expansion coefficient, $\boldsymbol{f}$ the external body forces, ϑ_0 the reference temperature, $\boldsymbol{g}$ the gravity acceleration vector, Q the heat source and $\boldsymbol{u}^0$ and ϑ^0 the initial conditions for velocity and temperature, respectively. For simplicity in the exposition, we have assumed homogeneous Dirichlet boundary conditions for both velocity and temperature.

The literature on the finite element approximation of problems (2.1-2.7) is vast (see for example, the introductory text Ready and Gartling 1994 [43]). The spatial discretization suffers from the well-known problems of compatibility conditions between the velocity and pressure finite element spaces as well as the instabilities due to convection dominated flows, in this case both in the

momentum equation (2.1) and the heat equation (2.3).

Apart from numerical difficulties, the physics modelled by Equations (2.1-2.7) is extremely complex. In particular, turbulence should be in principle modelled by this system of equations. Since it is commonly accepted that turbulent scales cannot be captured in most applications, turbulence models of different complexity have been developed (D.C. Wilcox 1993 [53]).

In recent years, the idea of using numerical techniques able to cope with the potential instabilities and to model turbulence at the same time has gained adepts, in particular within the variational multiscale concept introduced in Hughes 1995 [26], Hughes 1998 [49]. The original motivation of this type of formulation was to justify the so called stabilized finite element methods. The possibility to model turbulence was remarked in Codina2000 [10] by contrast with the option adopted in Hughes et al.2000 [50] to add a large-eddy-simulation (LES) type model for the subgrid scales (see Remark 6 in Codina2002 [13] and, for background on LES models S.B Pope 2000 [46]). In Bazilevs2007 [54] the possibility to model turbulence using only numerical ingredients within the variational multiscale context is fully and successfully exploited. The role of numerical stabilization terms to model turbulence had also been envisaged in de Sampio [18], Hoffman and Johnson 2006 [23], for example. For similar ideas using other numerical formulations, see Boris et al.1992 [29], Sagaut [45] and references therein.

2.2 Turbulence

Turbulence is that state of fluid motion which is characterized by apparently random and chaotic three-dimensional vorticity. When turbulence is present, it usually dominates all other flow phenomena and results in increased energy dissipation, mixing, heat transfer and drag. If there is no three-dimensional vorticity, there is no real turbulence. The reasons for this will become clear later; but briefly, it is the ability to generate new vorticity from old vorticity that is essential to turbulence. And only in a three-dimensional flow, is the necessary stretching and turning of vorticity by the flow itself possible. For more details about turbulence see William [21].

2.2.1 Complexity of the turbulence model

Complexity of different turbulence models may vary strongly depending on the details one wants to observe and investigate by carrying out such numerical simulations. Complexity is due to the nature of Navier-Stokes equation (N-S equation). N-S equation is inherently nonlinear, time-dependent, three-dimensional PDE.

Turbulence could be thought of as instability of laminar flow that occurs at high Reynolds number (Re). Such instabilities origin form interactions between non-linear inertial terms and viscous terms in N-S equation. These interactions are rotational, fully time-dependent and fully three-dimensional. Rotational and three-dimensional interactions are mutually connected via vortex stretching. Vortex stretching is not possible in two dimensional space. That is also why no satisfactory two-dimensional approximations for turbulent phenomena are available (see John et.al.2006 [51]).

Furthermore turbulence is thought of as random process in time. Therefore no deterministic approach is possible. Certain properties could be learned about turbulence using statistical methods. These introduce certain correlation functions among flow variables. However it is impossible to determine these correlations in advance. Another important feature of a turbulent flow is that vortex

structures move along the flow. Their lifetime is usually very long. Hence certain turbulent quantities cannot be specified as local. This simply means that upstream history of the flow is also of great importance (Sodja2007 [48]).

2.2.2 Turbulence production and dissipation

Turbulence is initially generated by instabilities in the flow caused by mean velocity gradients. These eddies in their turn breed new instabilities and hence smaller eddies. The process continues until the eddies become sufficiently small (and fluctuating velocity gradients sufficiently large) that viscous effects become significant and dissipate turbulence energy as heat see figure (2.1). This process the continual creation of turbulence energy at large scales, transfer of energy to smaller and smaller eddies and the ultimate dissipation of turbulence energy by viscosity is called the turbulent energy cascade (Apsley2004 [2]).

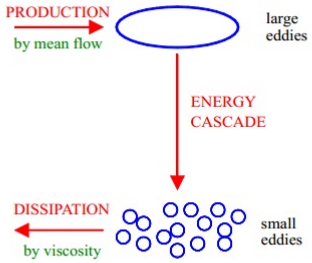

Fig. 2.1: Turbulence production and dissipation.

2.2.3 Classification of turbulence models

Nowadays turbulent flows may be computed using several different approaches. Either by solving the Reynolds-averaged Navier-Stokes equations with suitable models for turbulent quantities or by computing them directly. The main approaches of turbulence modeling can be summarized by these models.

- Reynolds Average Navier-Stokes (RANS) Models
- Large Eddy Simulations (LES)
- Direct Numerical Simulations (DNS)

Extension of modeling for certain CFD approach is illustrated in the following figure (2.2). It is clearly seen, that models computing fluctuation quantities resolve shorter length scales than models solving RANS equations. Hence they have the ability to provide better results. However they have a demand of much greater computer power than those models applying RANS methods(Bell2003 [5]).

Large eddy simulation are based on space-filtered equations. Time dependent calculations are performed and large eddies are explicitly calculated. For small eddies, their effect on the flow pattern is taken into account with a “subgrid model”of which many possibilities are available.

For Direct Numerical simulation large computational resource are required as all the eddies are numerically solved without any turbulence model.

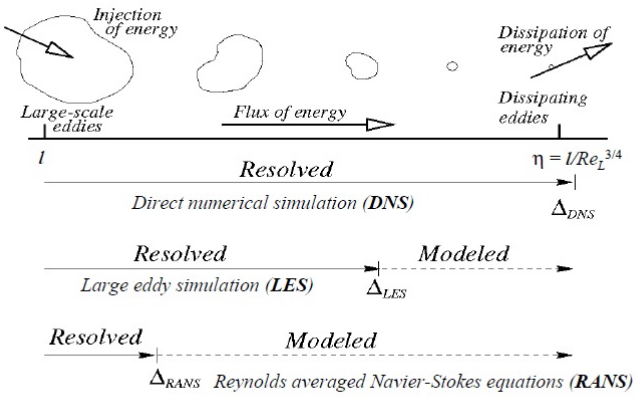

Fig. 2.2: Extend of modeling for certain types of turbulent models.

2.2.4 Reynolds Averaged Navier-Stokes (RANS) Models

The following section deals with the concept of Reynolds decomposition or Reynolds averaging. The term Reynolds stress is introduced and explained briefly by Saad [44]. Any property (whether a vector or a scalar) can be written as the sum of an average and a fluctuation. This decomposition will yield a set of equations governing the average flow field. The new equations will be exact for an average flow field not for the exact turbulent flow field. By an average flow field we mean that any property becomes constant over time. The result of using the Reynolds decomposition in the NS equations is called the RANS or Reynolds Averaged Navier Stokes Equations. Upon substitution of the Reynolds decomposition (for each variable, we substitute the corresponding decomposition) we obtain the following RANS equations. We start from the governing equation for the Newtonian fluid which are:
Conservation of Mass

$$\frac{\partial \rho}{\partial t} + \frac{\partial \rho u_i}{\partial x_i} = 0 \tag{2.8}$$

Conservation of momentum

$$\frac{\partial u_i}{\partial t} + \frac{\partial}{\partial x_j}(u_i u_j) = \frac{\partial}{\partial x_j}(\nu \frac{\partial u_i}{\partial x_j}) - \frac{1}{\rho}\frac{\partial p}{\partial x_i} \tag{2.9}$$

Where u_i is the instantaneous velocity. The velocity and pressure components can be decomposed as:

$$u_i = \bar{u}_i + u_i', \quad p = \bar{p} + p' \tag{2.10}$$

In turbulent flow we divide the instantaneous velocity u_i into a mean part $\bar{u}_i$(time-averaged part) and a fluctuating part u_i'. This is called Reynolds decomposition. The time-averaged velocity is obtained from

$$u_i' = \frac{1}{2\Delta T}\int_{-T}^{T} U(\tau)d\tau \tag{2.11}$$

Inserting equation 2.10 into equation 2.9, and since we have the following relations:

$$\overline{\bar{u}_i u_i'} = \bar{\bar{u}}\bar{u_i'} = 0, \quad \overline{\bar{u}_i + u_i'} = \bar{\bar{u}} + \bar{u_i'} = \bar{u} \tag{2.12}$$

and time averaging gives

$$\frac{\partial(\overline{\bar{u}_i + u_i'})}{\partial t} + \frac{\partial}{\partial x_j}[\overline{(\bar{u}_i + u_i')(\bar{u}_j + u_j')}] = \frac{\partial}{\partial x_j}[\nu \frac{\partial}{\partial x_j}(\overline{\bar{u}_i + u_i'})] - \frac{1}{\rho}\frac{\partial}{\partial x_i}(\overline{\bar{p} + p'}) \tag{2.13}$$

$$\frac{\partial \bar{u}_i}{\partial t} + \frac{\partial}{\partial x_j}[\overline{\bar{u}_i \bar{u}_j} + \overline{\bar{u}_j u_i'} + \overline{\bar{u}_i u_j'} + \overline{u_j' u_i'}] = \frac{\partial}{\partial x_j}[\nu \frac{\partial}{\partial x_j}(\overline{\bar{u}_i + u_i'})] - \frac{1}{\rho}\frac{\partial}{\partial x_i}(\overline{\bar{p} + p'}) \tag{2.14}$$

Using equation (2.12) the two terms on the right hand side of equation (2.14) can be written as

$$\frac{1}{\rho}\frac{\partial}{\partial x_i}(\overline{\bar{p} + p'}) = -\frac{1}{\rho}\frac{\partial \bar{p}}{\partial x_i}$$

$$\frac{\partial}{\partial x_j}[\nu \frac{\partial}{\partial x_j}(\overline{\bar{u}_i + u_i'})] = \frac{\partial}{\partial x_j}(\nu \frac{\partial \bar{u}_i}{\partial x_j})$$

The left hand side of equation (2.14) can, using equation (2.12) be written as:

$$\frac{\partial}{\partial x_j}[\overline{\bar{u}_i \bar{u}_j} + \overline{\bar{u}_j u_i'} + \overline{\bar{u}_i u_j'} + \overline{u_j' u_i'}] = \frac{\partial}{\partial x_j}[\overline{\bar{u}_i \bar{u}_j} + \overline{u_j' u_i'}]$$

using continuity equation $\frac{\partial}{\partial x_j}(\overline{\bar{u}_i \bar{u}_j}) = \bar{u}_i \frac{\partial \bar{u}_j}{\partial x_j} + \bar{u}_j \frac{\partial \bar{u}_i}{\partial x_j} = \bar{u}_j \frac{\partial \bar{u}_i}{\partial x_j}$, we can finally write the equation (2.14) as:

$$\frac{\partial \bar{u}_i}{\partial t} + \frac{\partial \bar{u}_i}{\partial x_j} = \frac{1}{\rho}\frac{\partial}{\partial x_j}(-\bar{p}\delta_{ij} + \mu \frac{\partial \bar{u}_i}{\partial x_j} - \rho \overline{u_j' u_i'}) \tag{2.15}$$

On the right hand side of equation (2.15) a new unknown term appears $-\rho \overline{u_j' u_i'}$ which can be regarded as an additional stress due to the decomposition. It is called a Reynolds stress. This term describes the diffusive nature of turbulence(see Socolofsky [47]). Since it is unknown, it must be modelled and we have to introduce different types of RANS turbulence modeling.

In figure (2.3) illustrates the different types of modeling approach by RANS.

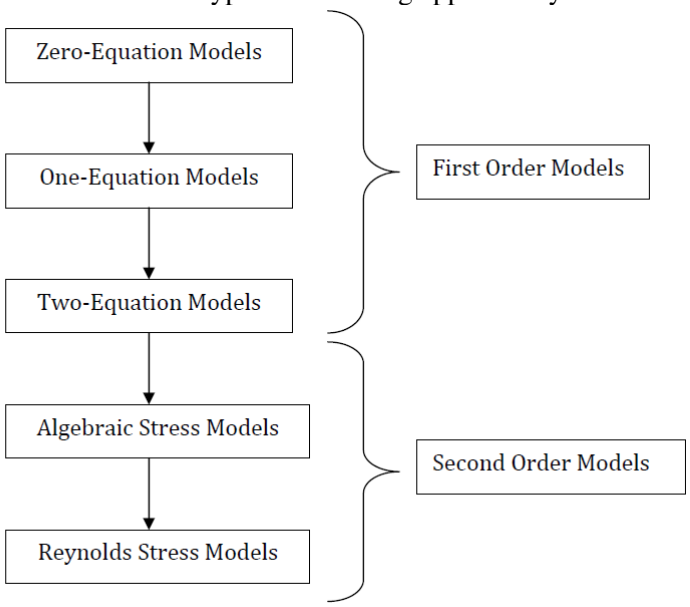

Fig. 2.3: RANS Turbulence Modeling.

1. **Linear eddy viscosity models**

These are turbulence models in which the Reynolds stresses, as obtained from a Reynolds averaging of the Navier-Stokes(RANS) equations, are modelled by a linear constitutive relationship with the mean flow straining field, as:

$$-\rho\left\langle\overline{u_i' u_j'}\right\rangle = 2\mu_t S_{ij} - \frac{2}{3}\rho k\delta_{ij} \tag{2.16}$$

where,$\langle\cdot\rangle$ defines the average advection of u_i' by u_j' and

- μ_t is the coefficient termed turbulence "viscosity"(also called the eddy viscosity).
- $k = \frac{1}{2}(\langle u_1 u_1\rangle + \langle u_2 u_2\rangle + \langle u_3 u_3\rangle)$ is the mean turbulent kinetic energy.
- $S_{ij} = \frac{1}{2}[\frac{\partial U_i}{\partial x_j} + \frac{\partial U_j}{\partial x_i}] - \frac{1}{2}\frac{\partial U_k}{\partial x_k}\delta_{\text{ij}}$ is the mean strain rate.

Note that inclusion of $\frac{2}{3}\rho k\delta_{ij}$ in the linear constitutive relation is required by tensorial algebra purposes when solving for two-equation turbulence models (or any other turbulence model that solves a transport equation for k). This linear relationship is also known as the Boussinesq hypothesis. There are several subcategories for the linear eddy-viscosity models, depending on the number of (transport) equations solved to compute the eddy viscosity coefficient.

(a) Algebric models

(b) One equation models

(c) Two equation models

(a) **Algebric Turbulence Models**

Algebraic turbulence models or zero-equation turbulence models are models that do not require the solution of any additional equations, and are calculated directly from the flow variables. As a consequence, zero equation models may not be able to properly account for history effects on the turbulence, such as convection and diffusion of turbulent energy. These models are often too simple for use in general situations, but can be quite useful for simple flow geometries or in start-up situations (e.g. the initial phases of a computation in which a more complicated model may have difficulties).

(b) **One Equation Turbulence Models**

One equation turbulence models solve one turbulent transport equation, usually the turbulent kinetic energy. The original one-equation model is Prandtl's one-equation model. Other common one-equation models are:

- Baldwin-Barth model
- Spalart-Allmaras model

The Spalart-Allmaras model is a one equation model for the turbulent viscosity. It solves a transport equation for a viscosity-like variable $\tilde{\nu}$ which may be referred to as the Spalart-Allmaras variable. The Spalart-Allmaras model was designed specifically for aerospace applications involving wall-bounded flows and has been shown to give good results for

boundary layers subjected to adverse pressure gradients. The one-equation model is given by the following equation:

$$\frac{\partial\tilde{\nu}}{\partial t}+u_j\frac{\partial\tilde{\nu}}{\partial x_j} = C_{b1}[1-f_{t2}]\tilde{S}\tilde{\nu}+\frac{1}{\sigma}\{\nabla\cdot[\nu+\tilde{\nu}]\nabla\tilde{\nu}+C_{b2}|\nu|^2\}-[C_{\omega1}f_\omega-\frac{C_{b1}}{\kappa^2}f_{t2}](\frac{\tilde{\nu}}{d})^2+f_{t1}\Delta U^2 \tag{2.17}$$

where the turbulent eddy viscosity is given by $\nu_t = \tilde{\nu}f_{v1}$, where $f_{v1} = \frac{\chi^3}{\chi^3+C_{b1}}$, $\chi := \frac{\tilde{\nu}}{\nu}$ and ΔU is the difference between the velocity at the field point and that at the trip (on the wall) Additional definitions are given by the following equations:

$$\tilde{S} = S + \frac{\tilde{\nu}}{\kappa_2 d_2}f_{v2},$$

$$f_{v2} = 1 - \frac{\chi}{1+\chi f_{v1}}$$

where

$$S = \sqrt{\Omega_{ij}\Omega_{ij}}$$

is the magnitude of the vorticity, d is the distance from the field point to the nearest wall, and

$$\Omega_{ij} = \frac{1}{2}(\frac{\partial u_i}{\partial x_j} - \frac{\partial u_j}{\partial x_i})$$

$$f_\omega = g[\frac{1+C_{\omega3}^6}{g^6+C_{\omega3}^6}]^{1/6}$$

$$g = r + C_{w2}(r^6 - r)$$

$$r = \frac{\tilde{\nu}}{\tilde{S}\kappa^2 d^2}$$

$$f_{t1} = C_{t1}g_t\exp(-C_{t2}\frac{\omega_t}{\Delta U^2}+{g_t}^2 d_t^2)$$

$$f_{t2} = C_{t3}\exp(-C_{t4}\chi^2)$$

where ω_t is the wall vorticity at the trip, d_t is the distance from the field point to the trip. The boundary conditions are: $\tilde{\nu}_{\text{wall}} = 0$, $\tilde{\nu}_{\text{farfield}} = 3\nu_\infty - 5\nu_\infty$.
The constants are:

$$\sigma = \frac{2}{3}, \quad C_{b1} = 0.1355, \quad C_{\text{b2}} = 0.622, \quad \kappa = 0.41, \quad C_{\omega1} = \frac{C_{b1}}{\kappa^2}+\frac{1+C_{b2}}{\sigma},$$
$$C_{\omega2} = 0.3, \quad C_{\omega3} = 2, \quad C_{v1} = 7.1, \quad C_{t1} = 1, \quad C_{t2} = 2, \quad C_{t3} = 1.1, \quad C_{t4} = 2$$

(c) **Two Equation Turbulence Models**

Two equation turbulence models are one of the most common type of turbulence models. Models like the k-epsilon($k-\epsilon$) model and the k-omega($k-\omega$) model have become industry standard models and are commonly used for most types of engineering problems. Two equation turbulence models are also very much still an active area of research and new refined two-equation models are still being developed.

By definition, two equation models include two extra transport equations to represent the turbulent properties of the flow. This allows a two equation model to account for history effects like convection and diffusion of turbulent energy.

Most often one of the transported variables is the turbulent kinetic energy, k. The second

transported variable varies depending on what type of two-equation model it is. Common choices are the turbulent dissipation, ϵ or the specific dissipation, ω. The second variable can be thought of as the variable that determines the scale of the turbulence (length-scale or time-scale), whereas the first variable, k determines the energy in the turbulence.

2. **Algebraic stress model**

Algebraic stress model(ASM) is a simplified Reynolds stress model. In the algebraic stress model, two main approaches can be undertaken. In the first, the transport of the turbulent stresses is assumed proportional to the turbulent kinetic energy; while in the second, convective and diffusive effects are assumed to be negligible. Algebraic Stress models can only be used where convective and diffusive fluxes are negligible, i.e. source dominated flows.

The Reynolds stress model(RSM) and $k-\epsilon$ models are written in a symbolic form as:

$$\text{RSM:} \quad C_{ij} - D_{ij} = P_{ij} + \Phi_{ij} - \epsilon_{ij}$$

$$k-\epsilon : C_k - D_k = P_k - \epsilon$$

The assumption in ASM is that the transport(convective and diffusive) of $\rho\overline{u_i' u_j'}$ is related to that k, i.e.

$$C_{ij} - D_{ij} = \frac{\rho\overline{u_i' u_j'}}{k}(C_k - D_k)$$

which gives:

$$\rho\overline{u_i' u_j'} = \frac{2}{3}\delta_{ij}k + \frac{k}{\epsilon}\frac{(1-c_2)(P_{ij} - \frac{2}{3}\delta_{ij}P) + \Phi'_{ij,1} + \Phi'_{ij,2}}{c_1 + P/\epsilon - 1}$$

where C_{ij} is convective term, D_{ij} is diffusion term, P_{ij} and P are the production term of $\rho\overline{u_i' u_j'}$ and k, Φ_{ij} is the pressure-strain correlation term which promotes isotropy of the turbulence and ϵ, ϵ_{ij} are dissipation (i.e. transformation of mechanical energy into heat in the small-scale turbulence) of k and $\rho\overline{u_i' u_j'}$ respectively(see Davidson.2005 [17]).

3. **Reynolds stress model**

The Reynolds stress model involves calculation of the individual Reynolds stresses $\rho\overline{u_i' u_j'}$, using differential transport equations. The individual Reynolds stresses are then used to obtain closure of the Reynolds-averaged momentum equation(see Davidson2005 [17]).

The exact transport equations for the transport of the Reynolds stresses $\rho\overline{u_i' u_j'}$, may be written as follows:

$$\begin{aligned}\frac{\partial}{\partial t}(\rho\overline{u_i' u_j'}) + \frac{\partial}{\partial x_k}(\rho\bar{u_k}\overline{u_i' u_j'}) = -\rho(\overline{u_i' u_k'}\frac{\partial \bar{u}_j}{\partial x_k} + \overline{u_j' u_k'}\frac{\partial \bar{u}_i}{\partial x_k}) \\ +\overline{p'(\frac{\partial u_i'}{\partial x_j} + \frac{\partial u_j'}{\partial x_i})} - \frac{\partial}{\partial x_k}[\rho\overline{u_i' u_j' u_k'} + \overline{p'(u_j'\delta_{ik})} + \overline{p'(u_i'\delta_{jk})} - \nu\frac{\partial}{\partial x_k}(\overline{u_i' u_j'})] \\ - 2\nu\overline{\frac{\partial u_i'}{\partial x_k}\frac{\partial u_j'}{\partial x_k}}\end{aligned} \tag{2.18}$$

where

(a) $C_{ij} = \frac{\partial}{\partial x_k}(\rho\bar{u_k}\overline{u_i{'}u_j{'}})$ is the convective term,

(b) $P_{ij} = -\rho(\overline{u_i{'}u_k{'}}\frac{\partial\bar{u}_j}{\partial x_k} + \overline{u_j{'}u_k{'}}\frac{\partial\bar{u}_i}{\partial x_k})$ is the production term,

(c) $\Phi_{ij} = \overline{p'(\frac{\partial u_i'}{\partial x_j} + \frac{\partial u_j'}{\partial x_i})}$ is the pressure-strain correlation term,

(d) $D_{ij} = -\frac{\partial}{\partial x_k}[\rho\overline{u_i{'}u_j{'}u_k{'}} + \overline{p'(u_j'\delta_{ik})} + \overline{p'(u_i'\delta_{jk})} - \nu\frac{\partial}{\partial x_k}(\overline{u_i'u_j'})]$ is the diffusion term,

(e) $\epsilon_{ij} = 2\nu\overline{\frac{\partial u_i'}{\partial x_k}\frac{\partial u_j'}{\partial x_k}}$ is the dissipation term.

which symbolically can be written as:

$$\text{Local time derivative} + C_{ij} - D_{ij} = P_{ij} + \Phi_{ij} - \epsilon_{ij}$$

The objective is to find models for turbulent diffusion (D_{ij}), the pressure strain correlation Φ_{ij} and the turbulent dissipation rate ϵ_{ij}(Saad [44]).

2.2.5 Large Eddy Simulation

Large eddy simulation (LES) is a popular technique for simulating turbulent flows. An implication of Kolmogorov's (1941) theory of self similarity is that the large eddies of the flow are dependant on the geometry while the smaller scales are more universal. This feature allows one to explicitly solve for the large eddies in a calculation and implicitly account for the small eddies by using a subgrid-scale model (SGS model).

Mathematically, one may think of separating the velocity field into a resolved and sub-grid part. The resolved part of the field represents the "large-scales"eddies, while the subgrid part of the velocity represents the "small-scales"whose effect on the resolved field is included through the subgrid-scale model. Formally, one may think of filtering as the convolution of a function with a filtering kernel G.

$$\bar{u_i}(\vec{x}) = \int G(\vec{x} - \vec{\xi})u(\vec{\xi})d\vec{\xi} \tag{2.19}$$

resulting in $u_i = \bar{u_i} + u_i'$
where $\bar{u_i}$ is the resolvable scale part and u_i' is the subgrid-scale part. However, most practical (and commercial) implementations of LES use the grid itself as the filter (the box filter) and perform no explicit filtering. The filtered equations are developed from the incompressible Navier-Stokes equations of motion:

$$\frac{\partial u_i}{\partial t} + u_j\frac{\partial u_i}{\partial x_j} = -\frac{1}{\rho}\frac{\partial p}{\partial x_i} + \frac{\partial}{\partial x_j}(\nu\frac{\partial u_i}{\partial x_j}) \tag{2.20}$$

Substituting in the decomposition $u_i = \bar{u_i} + u_i'$ and $p = \bar{p} + p'$ and then filtering the resulting equation gives the equations of motion for the resolved field:

$$\frac{\partial\bar{u_i}}{\partial t} + \bar{u_j}\frac{\partial\bar{u_i}}{\partial x_j} = -\frac{1}{\rho}\frac{\partial\bar{p}}{\partial x_i} + \frac{\partial}{\partial x_j}(\nu\frac{\partial\bar{u_i}}{\partial x_j}) + \frac{1}{\rho}\frac{\partial\tau_{ij}}{\partial x_i} \tag{2.21}$$

The extra term $\frac{\partial\tau_{ij}}{\partial x_i}$ arises from the non-linear advection terms, due to the fact that

$$\overline{u_j\frac{\partial u_i}{\partial x_j}} \neq \bar{u_j}\frac{\partial\bar{u_i}}{\partial x_j} \tag{2.22}$$

and hence

$$\tau_{ij} = \bar{u_i}\bar{u_j} - \overline{u_iu_j} \tag{2.23}$$

Similar equations can be derived for the subgrid-scale field (i.e. the residual field). Subgrid-scale turbulence models usually employ the Boussinesq hypothesis, and seek to calculate (the deviatoric part of) the SGS stress using:

$$\tau_{ij} - \frac{1}{3}\tau_{kk}\delta_{ij} = -2\mu_t \bar{S_{ij}} \tag{2.24}$$

where $\bar{S_{ij}}$ is the rate-of-strain tensor for the resolved scale defined by

$$\bar{S_{ij}} = \frac{1}{2}(\frac{\partial \bar{u_i}}{\partial x_j} + \frac{\partial \bar{u_j}}{\partial x_i})$$

and ν_t is the subgrid-scale turbulent viscosity. Substituting into the filtered Navier-Stokes equations, we then have:

$$\frac{\partial \bar{u_i}}{\partial t} + \bar{u_j}\frac{\partial \bar{u_i}}{\partial x_j} = -\frac{1}{\rho}\frac{\partial \bar{p}}{\partial x_i} + \frac{\partial}{\partial x_j}(\nu \frac{\partial \bar{u_i}}{\partial x_j}) + \frac{\partial}{\partial x_j}([\nu + \nu_t]\frac{\partial \bar{u_i}}{\partial x_j}) \tag{2.25}$$

where we have used the incompressibility constraint to simplify the equation and the pressure is now modified to include the trace term $\tau_{kk}\delta_{ij}/3$.

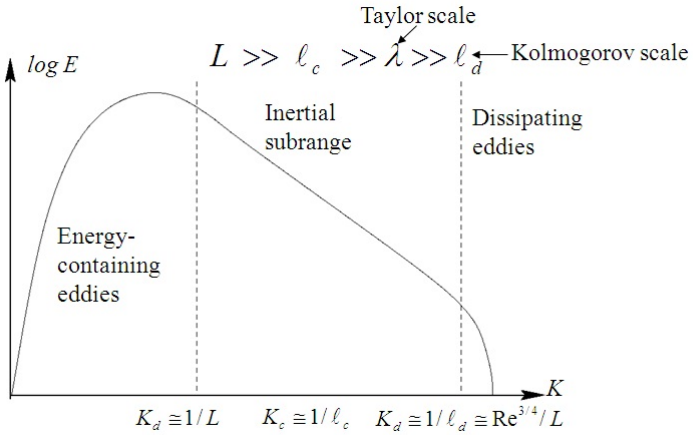

Fig. 2.4: Energy Cascade of Kolmogorov spectrum

From the figure (2.4) it is visible that the energy cascade of LES turbulence modeling using Kolmogorov spectrum. Energy spectrum for LES, means that we have to consider the energy of large eddies plus the energy of subgrid scale. To find the energy for subgrid scale we have to derive it from Kolmogorov hypothesis, which means that for eddies much smaller than the energy containing eddies and much larger that dissipative eddies (of the order of Kolmogorov scales), turbulence is controlled solely by the dissipation rate (ϵ) and the size of the eddy ($\frac{1}{k}$), where k is the wave number and equals $\frac{1}{L}$ (L=size of eddies). In this subrange turbulent energy spectrum $E(k)$ is a Kolmogorov spectrum i.e.

$$E(k) = K_0 \epsilon^{2/3} k^{-5/3}, \quad k \in [0, \infty] \tag{2.26}$$

where K_0 is the Kolmogorov constant and ϵ the kinetic energy dissipation rate. The goal of Large Eddy Simulation is to resolve part of the inertial range. Here we will discuss about Smagorinsky Model.

The Smagorinsky Model is based on the large scales. It is generally used in a local form for the physical space, i.e. variable in space, in order to be more adaptable to the flow being calculated. It is obtained by space and time localization of the statistical relations. There is no particular justification for this local use of relations that are on average true for the whole, since they only ensure that the

energy transfer through the cutoff are expressed correctly on the average not locally. This model is expressed as:

$$\nu_{\text{sgs}}(\boldsymbol{x}, t) = (C_s\bar{\Delta})^2(2|\bar{S}(\boldsymbol{x}, t)|^2)^{1/2} \tag{2.27}$$

where $\bar{\Delta}$ is the grid size and the constant C_s is evaluated by the relation

$$C_s = \frac{1}{\pi}(\frac{3K_0}{2})^{-3/4} \sim 0.18$$

It should nonetheless be noted that the value of this constant C_s is adjusted to improve the solution. The Smagorinsky constant usually has the value $C_s \simeq 0.1 - 0.2$ and $\bar{S} = \sqrt{2\bar{S}_{\text{ij}}\bar{S}_{\text{ij}}}$. See Saugat2001 [45] for more details about Smagorinsky model.

2.2.6 Direct Numerical Simulation

A direct numerical simulation (DNS) is a simulation in computational fluid dynamics in which the Navier-Stokes equations are numerically solved without any turbulence model. This means that the whole range of spatial and temporal scales of the turbulence must be resolved. All the spatial scales of the turbulence must be resolved in the computational mesh, from the smallest dissipative scales (Kolmogorov scales), up to the integral scale L, associated with the motions containing most of the kinetic energy. The Kolmogorov scale, η is given by

$$\eta = (\nu^3/\epsilon)^{1/4}$$

where ν is the kinematic viscosity and ϵ is the rate of kinetic energy dissipation. On the other hand, the integral scale depends usually on the spatial scale of the boundary conditions. To satisfy these resolution requirements, the number N of points along a given mesh direction with increments h, must be

$$Nh > L$$

so that the integral scale is contained within the computational domain, and also $h \leqslant \eta$ so that the Kolmogorov scale can be resolved. Since $\varepsilon \approx {u'}^3/L$ where u' is the root mean square (RMS) of the velocity, the previous relations imply that a three-dimensional DNS requires a number of mesh points N^3 satisfying $N^3 \geqslant Re^{9/4}$ where Re is the turbulent Reynolds number $Re = \frac{u'L}{\nu}$

Hence, the memory storage requirement in a DNS grows very fast with the Reynolds number. In addition, given the very large memory necessary, the integration of the solution in time must be done by an explicit method except for the pressure which needs to be treated implicitly. This means that in order to be accurate, the integration must be done with a time step, Δt small enough such that a fluid particle moves only a fraction of the mesh spacing h in each step. That is, $C = \frac{u'\Delta t}{h} < 1$ where C is the courant number. The total time interval simulated is generally proportional to the turbulence time scale τ given by $\tau = L/u'$. Combining these relations, and the fact that h must be of the order of η, the number of time-integration steps must be proportional to $L/(C\eta)$. By other hand, from the definitions for Re, η and L given above, it follows that $\frac{L}{\eta} \sim Re^{3/4}$ and consequently, the number of time steps grows also as a power law of the Reynolds number. One can estimate that the number of floating-point operations required to complete the simulation is proportional to the number of mesh points and the number of time steps, and in conclusion, the number of operations grows as Re^3.

Therefore, the computational cost of DNS is very high, even at low Reynolds numbers. For the Reynolds numbers encountered in most industrial applications, the computational resources required

by a DNS would exceed the capacity of the most powerful computer currently available. However, direct numerical simulation is a useful tool in fundamental research in turbulence. Using DNS it is possible to perform "numerical experiments", and extract from them information difficult or impossible to obtain in the laboratory, allowing a better understanding of the physics of turbulence. Also, direct numerical simulations are useful in the development of turbulence models for practical applications, such as sub-grid scale models for Large eddy simulation (LES) and models for methods that solve the Reynolds-averaged Navier-Stokes equations (RANS). This is done by means of "a priori"tests, in which the input data for the model is taken from a DNS simulation, or by "a posteriori"tests, in which the results produced by the model are compared with those obtained by DNS(see Orszag1970 [35] and Yokokawa et.al.2002 [33]).

Chapter 3

Numerical approximation of the convection-diffusion equation

In this Chapter an overview of the finite element approximation of the convection-diffusion equation is presented. The three main aspects of this chapter are, the global stabilization in the convective dominated regime, the treatment of the local instabilities that still remain close to layers when a stabilized formulation is used and the way to deal with transient problems.

3.1 Introduction

The starting point of our formulation is the variational multiscale framework. The main idea is to split the unknown into a finite element component and a remainder that is assumed that the finite element mesh cannot resolve. A closed form expression is then proposed for this remainder, referred to as subgrid-scale. When inserted into the equation for the finite element component, a method with enhanced stability properties is obtained. In our approach, we take the space for the subgrid-scales orthogonal to the finite element space.

Once global instabilities have been overcome, there are still local oscillations near layers due to the lack of monotonicity of the method. Shock capturing technique are often employed to deal with them. Here, our point of view is that this lack of monotonicity is inherent to the integral as duality pairing intrinsic to the variational formulation of the problem. Shock capturing techniques can resolute the sharp gradients without any local oscillations in numerical solutions.

The final point we discussed is the stabilized formulation of time-dependent problems in convection-diffusion equation. We mainly chose the subgrid scale(SGS) for this time dependent problem as time dependent and orthogonal to the finite element space to see how the dissipative structure and energy transfer mechanism works between two scales.

3.2 Multiscale approximation of the convection-diffusion-reaction equation

The objective of this section is to summarize the basic stabilized finite element method we use to solve the convection-diffusion-reaction equation (CDRE) in the case in which diffusion is small, that is to say, convective effects are dominant. It is not our intention here neither to describe the details of the problem, which are well known, not to give a fair acknowledgement of the key contributions to design the final method that can be found in the literature. This is why, apart from our own work,

only reference to the landmark paper by Hughes1995 [26] and a book chapter of Codina2001 from [7] are mentioned.

Let us start with the problem we are interested in. For the purposes of this section it is enough to consider the stationary CDRE with homogeneous Dirichlet boundary conditions. The problem consists of finding u such that

$$\mathcal{L}u := -k\Delta u + \boldsymbol{a}\cdot\nabla u + su = f \quad \text{in} \quad \Omega$$

$$u = 0 \quad \text{on} \quad \partial\Omega$$

where $k > 0$ is the diffusion coefficient, $s \geqslant 0$ the reaction coefficient, $\boldsymbol{a} \in \mathbb{R}^d$ is the advection coefficient and f is a given datum. The problem is posed in the domain $\Omega \subset \mathbb{R}^d (d = 2, 3)$. Constant coefficients will be assumed throughout, for the sake of conciseness.

The variational form of the problem can be written as follows: find $u \in V = H_0^1(\Omega)$ such that

$$B(u, v) = \langle f, v\rangle \quad \forall v \in V \tag{3.1}$$

where:

$$B(u, v) = k(\nabla u, \nabla v) + (\boldsymbol{a}\cdot\nabla u, v) + (su, v)$$

As usual $(\cdot,\cdot)$ denotes the L^2 inner product and $\langle\cdot,\cdot\rangle$ the integral of the product of two functions, including the duality pairing.

The conforming Galerkin finite element approximation of the problem is standard. If $V \subset V_h$ is a finite element space to approximate V, it consists of finding $u_h \in V_h$ such that

$$B(u_h, v_h) = \langle f, v_h\rangle \quad \forall v_h \in V_h$$

Again for simplicity, we will consider that the finite element partition associated to V_h is uniform, h being the size of the element domains.

It is well known that this formulation lacks stability when k is small. To justify the method we propose, it is interesting to start trying to elucidate which is the stability it has with some more detail than what is usual. If we take $v_h = u_h$ it is readily seen that

$$B(u_h, u_h) = k\|\nabla u_h\|^2 + s\|u_h\|^2 \tag{3.2}$$

The question is, what control, if any, can be obtained over the convective term? That is to say, is it possible to have a bound for $\|\boldsymbol{a}\cdot\nabla u_h\|$. To answer this fundamental question, we may obtain an improved stability estimate for the Galerkin method in the form of an inf-sup condition. If we take the test function as $v_{h,0} = \tau P_h(\boldsymbol{a}\cdot\nabla u_h)$, with the parameter τ to be defined and P_h being the projection onto V_h, we obtain:

$$\begin{aligned} B(u_h, v_{h,0}) \gtrsim \tau\|P_h(\boldsymbol{a}\cdot\nabla u_h)\|^2 &- k\|\nabla u_h\|\frac{C_{\text{inv}}}{h}\tau\|P_h(\boldsymbol{a}\cdot\nabla u_h)\| \\ &- s\|u_h\|\tau\|P_h(\boldsymbol{a}\cdot\nabla u_h)\| \end{aligned}$$

where $\gtrsim$ stands for $\geqslant$ up to positive constants and C_{inv} is the constant in standard inverse inequalities. If the parameter τ is chosen such that $\tau \leqslant \min\{\frac{h^2}{C_{inv}^2 k}, \frac{1}{s}\}$ then

$$B(u_h, v_{h,0}) \gtrsim \tau\|P_h(\boldsymbol{a}\cdot\nabla u_h)\|^2 - k\|\nabla u_h\|^2 - s\|u_h\|^2$$

The last two terms can be controlled, according to (3.2). It is then easily seen that $B(u_h, v_h) \gtrsim k\|\nabla u_h\|^2 + s\|u_h\|^2 + \tau\|P(\boldsymbol{a}\cdot\nabla u_h)\|^2$ with $v_h = u_h + \beta v_{h,0}$ where, $\beta > 0$ (β sufficiently small), and that with $k\|\nabla v_{h,0}\|^2 + s\|v_{h,0}\|^2 + \tau\|P_h(\boldsymbol{a}\cdot\nabla v_{h,0})\|^2 \lesssim \tau\|P_h(\boldsymbol{a}\cdot\nabla u_h)\|^2$, from where an inf-sup condition follows. Therefore, we may conclude that only control over $\tau\|P_h^{\perp}(\boldsymbol{a}\cdot\nabla u_h)\|^2$ is missing, with $P_h^{\perp} = I - P_h$, the projection orthogonal to the finite element space. This control is, at least, what any stabilized method must provide.

Let us describe now the formulation we propose. It is based on the splitting of the unknown u in a component u_h which can be resolved by the finite element space, and a remainder, that will be called subgrid scale (SGS). An approximation for the SGS is required to define a particular numerical formulation. The framework used here based on the formulation used in Hughes1995 [26]. Let $V = V_h \oplus \tilde{V}$, where $\tilde{V}$ is the space for the SGS. Then problem (3.1) unfolds into two variational equations in which we are looking for $u_h \in V_h$ and $\tilde{u} \in \tilde{V}$ such that

$$B(u_h, v_h) + B(\tilde{u}, v_h) = \langle f, v_h\rangle \quad \forall v_h \in V_h$$

$$B(u_h, \tilde{v}) + B(\tilde{u}, \tilde{v}) = \langle f, \tilde{v}\rangle \quad \forall \tilde{v} \in \tilde{V}$$

Here suppose that $\tilde{V}$ is made of smooth functions (which are anyhow dense in the complement of V_h). Then we may write:

$$B(u_h, v_h) + \langle \tilde{u}, \mathcal{L}^* v_h\rangle = \langle f, v_h\rangle \quad \forall v_h \in V_h \tag{3.3}$$

$$\langle \mathcal{L}u_h, \tilde{v}\rangle + \langle \mathcal{L}\tilde{u}, \tilde{v}\rangle = \langle f, \tilde{v}\rangle \quad \forall \tilde{v} \in \tilde{V} \tag{3.4}$$

where second derivatives applied to finite element functions have to be understood in the sense of distributions. The problem now can be stated as: how do we can model $\tilde{u}$? At this point is where approximations are required and different methods may be devised according to the approximation chosen.

The first approximation we shall choose is that:

$$\langle \mathcal{L}v_h, \tilde{v}\rangle \approx \sum_K (\mathcal{L}v_h, \tilde{v})_K \equiv (\mathcal{L}v_h, \tilde{v})_h \tag{3.5}$$

This essentially means that jumps of derivatives of finite elements functions across edges of the mesh are neglected. We shall stick to this assumption, although it can be relaxed, as explained in Codina et al.2009 [39].

The second approximation, which is definitely the most crucial, is:

$$\langle \mathcal{L}\tilde{u}, \tilde{v}\rangle \approx \tau^{-1}(\tilde{u}, \tilde{v}) \quad where \quad \tau^{-1} = c_1\frac{k}{h^2} + c_2\frac{|a|}{h} + c_3 s \tag{3.6}$$

where c_1, c_2 and c_3 are numerical parameters. There are many ways to arrive at this expression, which we shall not describe here. For an overview, see Codina1998 [14].

Equation (3.6) can be understood as a lumping of the equation for the SGS. This lumping is needed to make this equation directly solvable, without the need to introduce additional degrees of freedom into the problem. Both (3.5) and (3.6) can be justified from an approximate Fourier analysis requiring $\tau^{-1} \approx \|\mathcal{L}\|$ see Codina2002 [13]. Having introduced them, the final problem to be solved is:

$$B(u_h, v_h) + (\tilde{u}, \mathcal{L}^* v_h)_h = \langle f, v_h\rangle \quad \forall v_h \in V_h \tag{3.7}$$

$$(\mathcal{L}u_h, \tilde{v})_h + \tau^{-1}(\tilde{u}, \tilde{v}) = \langle f, \tilde{v}\rangle \quad \forall \tilde{v} \in \tilde{V} \tag{3.8}$$

which has to be compared with (3.3 - 3.4).

At this point we may already check which is the stability of the two scales introduced, namely, u_h and $\tilde{u}$ from Codina2001 [7]. From there we can say that we have the same control on the finite element component as for the Galerkin method *plus additional L^2 control on the* SGS.

The SGS is so far undefined. To choose the subspace $\tilde{V}$ we consider non-conforming approximations and $\tilde{V}$ might not be a subspace of $H_0^1(\Omega)$ see Codina2009 [39]. If $\tilde{P}$ is the L^2 projection to $\tilde{V}$, we have from (3.8) that

$$\tilde{u} = \tau\tilde{P}(f - \mathcal{L}u_h)$$

There are two obvious options:

- Choice I:
$$\tilde{V} \subset \mathcal{L}\,V_h + span\{f\} \Leftrightarrow \tilde{u} = \tau(f - \mathcal{L}u_h)$$
In this case, $\tilde{P}$ is the identity when applied to the finite element residual $f - \mathcal{L}u_h$. This option is the most common in the literature. It is known as *Algebraic subgrid scale approximation*(ASGS) proposed in Codina2000 [9]. It yields a stable formulations, as we shall see. From the conceptual point of view, the danger it has is that the assumption $V_h \cap \tilde{V} = \{0\}$, crucial to derive the method, may not hold.

- Choice II:
$$\tilde{V} = V_h^{\perp} \Leftrightarrow \tilde{u} = \tau P_h^{\perp}(f - \mathcal{L}u_h)$$
This option was proposed in Codina2000 [9] which is known as *Orthogonal sub-scales*(OSS). In fact, it can be shown that if the SGS are further approximated as
$$\tilde{u} = -\tau P_h^{\perp}(\boldsymbol{a}\cdot\nabla u_h) \tag{3.9}$$
the method keeps the order of accuracy. Some care is needed though in the treatment of boundary effects.

Once the two choices have been described, let us write down the final finite element problem to be solved and obtain a simple stability estimate. For choice I the final problem is

$$B(u_h, v_h) + \tau(\mathcal{L}u_h, -\mathcal{L}^*v_h)_h = \langle f, v_h\rangle + \tau(f, -\mathcal{L}^*v_h)_h$$

It is immediately checked that

$$B(u_h, u_h) + \tau(\mathcal{L}u_h, -\mathcal{L}^*u_h)_h \gtrsim k\|\nabla u_h\|^2 + s\|u_h\|^2 + \tau\|(\boldsymbol{a}\cdot\nabla u_h)\|^2$$

Therefore, this method provides control over the whole convective term.
For choice II the finite element problem is

$$B(u_h, v_h) + \tau(P_h^{\perp}(\boldsymbol{a}\cdot\nabla u_h), P_h^{\perp}(\boldsymbol{a}\cdot\nabla v_h))_h = \langle f, v_h\rangle$$

and now we have that

$$B(u_h, u_h) + \tau(P_h^{\perp}(\boldsymbol{a}\cdot\nabla u_h), P_h^{\perp}(\boldsymbol{a}\cdot\nabla u_h))_h \gtrsim k\|\nabla u_h\|^2 + s\|u_h\|^2 + \tau\|P_h^{\perp}(\boldsymbol{a}\cdot\nabla u_h)\|^2$$

Thus, this simple stability estimate shows that the method provides control *only in the component of the convective term orthogonal to the finite element space*. However, $\tau\|P_h^{\perp}(\boldsymbol{a}\cdot\nabla u_h)\|^2$ *is precisely*

what the Galerkin method lacks. It is not difficult to foresee that one can in fact obtain optimal stability with choice II.

The results of the numerical analysis of the formulations arising both from choice I and from choice II is summarized next. Let:

$$|||v|||^2 := k\|\nabla v\|^2 + s\|v\|^2 + \tau\|(\boldsymbol{a}\cdot\nabla v)\|^2$$

$$E(h)^2 := (\frac{k}{h^2} + \frac{|\boldsymbol{a}|}{h} + s)h^{2(p+1)}|u|^2_{p+1} \approx \tau^{-1}h^{2(p+1)}|u|^2_{p+1}$$

where $|u|_{p+1}$ is the H^{p+1} seminorm of the exact solution u. If B_{stab} is the bilinear form of any of the two stabilized method introduced then it holds:

$$\inf_{u_h\in V_h}\sup_{v_h\in V_h}\frac{B_{\text{stab}}(u_h,v_h)}{|||u_h|||\,|||v_h|||} \geqslant C>0 \quad \text{Stability}$$

$$|||u-u_h||| \lesssim E(h) \quad \text{Optimal convergence}$$

From these results, there are some remarks to be made:

- The stability and convergence estimates presented are optimal.
- These estimates remain meaningful for all values of the physical parameters, which is the main goal of stabilized finite element methods.
- There is no need to refer to "$h^{p+1/2}$"estimation.

3.3 Shock capturing techniques

The methods proposed in the previous section yield stability and convergence in global norms. However, local oscillations may still remain in regions where the solution exhibits sharp layers. Even though these oscillations might be considered acceptable in linear problems, in nonlinear situations they may lead to a global failure of iterative schemes. Therefore, eliminating them in linear problems is a required step to extend the formulation to nonlinear equations. Methods aiming to avoid these local oscillations are often termed "*shock capturing*"or "*discontinuity capturing*"(DC) techniques.
To start, let us describe the guidelines to design DC methods as presented in Codina1993 [8] and references therein. Suppose that $s=0$ and let

$$\boldsymbol{a}_{\|} = \frac{\boldsymbol{a}\cdot\nabla u_h}{|\nabla u_h|} \quad \text{if} \quad |\nabla u_h|\neq 0, \quad \boldsymbol{a}_{\|}=0 \quad \text{otherwise}$$

The following observations are crucial:

- For regular P_1 elements, the discrete maximum principle (DMP) holds if an artificial diffusion K_{art} is added, which is the form of:

$$K_{\text{art}} = \frac{1}{2}\alpha h|\boldsymbol{a}_{\|}|, \quad \alpha \geqslant C - \frac{1}{Pe_{\|}} \quad \text{where} \quad Pe_{\|} = \frac{|\boldsymbol{a}_{\|}|h}{2k} \tag{3.10}$$

  where C is a constant that depends on the shape of the elements.
- If the DMP holds, L^∞ stability can be proved.
- If a numerical scheme is *linear* then it is at most first order accurate in L^∞ (a reformulation of Godunov's Theorem).

In view of these facts, DC methods may be designed trying to satisfy the DMP, at least in some simple situations, and need to be *nonlinear*. Three different types of shock or discontinuity capturing technique will be proposed here.

- Isotropic Residual Based Shock Capturing
- Anisotropic Residual Based Shock Capturing
- Orthogonal Projection Gradient Based Shock Capturing

3.3.1 Isotropic Residual Based Shock Capturing

The first family of DC methods proposed is that in which an artificial diffusion depending on the finite element residual is added to the basic stabilized formulation. The essential idea of this isotropic residual based shock capturing technique is *to design the artificial diffusion is a similar way like (3.10) but capturing k_{art} with*

$$\frac{|R(u_h)|}{|\nabla u_h|} \quad \text{instead of} \quad \boldsymbol{a}_{\|} = \frac{\boldsymbol{a}\cdot\nabla u_h}{|\nabla u_h|}$$

where $R(u_h) = f - \mathcal{L}u_h = f - (-k\Delta u_h + \boldsymbol{a}\cdot\nabla u_h + su_h)$ ($s \geqslant 0$ may be considered now). The resulting method is consistent, in the sense that if it is applied to the exact solution u the residual is zero.
The semilinear form of the problem is:

$$B_{\text{dc}}(u_h, v_h) = B_{\text{stab}}(u_h, v_h) + \sum_K (k_{\text{dc}}\nabla u_h, \nabla v_h)_K \tag{3.11}$$

with

$$k_{\text{dc}} = \frac{1}{2}\alpha h\frac{|R(u_h)|}{|\nabla u_h|} \tag{3.12}$$

This discontinuity diffusion will be added in all directions.

3.3.2 Anisotropic Residual Based Shock Capturing

A refinement of isotropic residual based shock capturing will be discussed here. We will try now to use previous idea of isotropic residual based shock capturing technique to introduce an anisotropic diffusion to eliminate oscillation near boundaries, both those due to convection and reaction. For consistency new dissipation added must be proportional to the element residual and for accuracy, it must vanish quickly in regions where the solution is smooth and also where the convective term in the residual is small.

The idea is that the diffusion introduced by the basic stabilization method can be shown to satisfy the requirements posed by the DMP (in some model cases), but it is only introduced along the streamlines. Therefore, k_{art} needs to be added only in the crosswind direction. This is accomplished by adding a diffusive term with the diffusion tensor.

$$\boldsymbol{k}_{\text{dc}} = \frac{1}{2}\alpha h\frac{|R(u_h)|}{|\nabla u_h|}(\boldsymbol{I} - \frac{\boldsymbol{a}\otimes\boldsymbol{a}}{|\boldsymbol{a}|^2})$$

to the basic stabilized finite element method, $\boldsymbol{I}$ being the second order identity tensor. From the expression of τ and α above in terms of upwind function it follows that CD will be always smaller

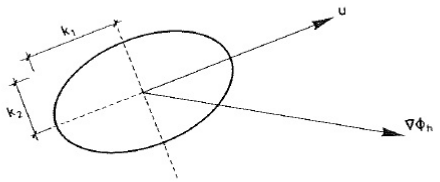

Fig. 3.1: Total diffusion ellipsoid. The values of k_1 and k_2 are $k_1 = k + \alpha h|u|/2$, $k_2 = k + \alpha_c h|R(u_h)|/2|\nabla u_h|$.

than the streamline diffusion introduced by SUPG formulation. The total diffusion ellipsoid in 2D is schematically represented by the figure(3.1).

3.3.3 Orthogonal Projection Gradient Based Shock Capturing

Following the guidelines to design DC methods discussed above, a different possibility to make the method consistent while introducing additional diffusion is to make it proportional to the projection of the gradient orthogonal to the finite element space. Thus, if k_{art} is the diffusion to be added, in order to make it active only in regions of sharp gradients *which cannot be resolved by the finite element mesh*, it can be multiplied by

$$\frac{|P_h^{\perp}(\nabla u_h)|}{|\nabla u_h|} \tag{3.13}$$

The semilinear form of the resulting problem is again (3.11), but now with k_{dc} given by

$$k_{\text{dc}} = \frac{1}{2}\alpha(|\boldsymbol{a}|h + sh^2)\frac{|P_h^{\perp}(\nabla u_h)|}{|\nabla u_h|}$$

Instead of (3.12). This artificial diffusion known as orthogonal projection of gradient based shock capturing will be added isotropically. Note that, apart from the factor (3.13), the artificial diffusion in this method is taken as $\frac{1}{2}\alpha(|\boldsymbol{a}|h + sh^2)$ independent of the finite element solution. As in the residual based DC methods, this diffusion can be introduced only in the streamline direction. It can resolute sharp gradients without local oscillations.

3.4 Time dependent convection-diffusion equation

Let us move our attention now to time dependent problems. The statement of the initial and boundary problem we are interested in is:

$$\partial_t u + \mathcal{L}u = f \quad \text{in} \quad \Omega, t > 0$$

$$u = 0 \quad \text{on} \quad \delta\Omega, t > 0$$

$$u = u^0 \quad \text{in} \quad \Omega, t = 0$$

Our approach consists in extending the scale splitting introduced in Section (3.2) to this problem. The time dependent counterpart of equation (3.3 - 3.4) is

$$(\partial_t u_h + \partial_t \tilde{u}, v_h) + B(u_h, v_h) + \langle \tilde{u}, \mathcal{L}^* v_h \rangle = \langle f, v_h \rangle \quad \forall v_h \in V_h$$

$$(\partial_t u_h + \partial_t \tilde{u}, \tilde{v}) + \langle \mathcal{L} u_h, \tilde{v} \rangle + \langle \mathcal{L} \tilde{u}, \tilde{v} \rangle = \langle f, \tilde{v} \rangle \quad \forall \tilde{v} \in \tilde{V}$$

The approximations used to arrive at (3.7 - 3.8) now lead to

$$(\partial_t u_h + \partial_t \tilde{u}, v_h) + B(u_h, v_h) + (\tilde{u}, \mathcal{L}^* v_h)_h = \langle f, v_h \rangle \quad \forall v_h \in V_h$$

$$(\partial_t u_h + \partial_t \tilde{u}, \tilde{v}) + (\mathcal{L} u_h, \tilde{v})_h + \tau^{-1}(\tilde{u}, \tilde{v}) = \langle f, \tilde{v} \rangle \quad \forall \tilde{v} \in \tilde{V}$$

If the space of SGS is chosen as orthogonal to the finite element space and approximation (3.9) is used, the problem to be solved becomes

$$(\partial_t u_h, v_h) + B(u_h, v_h) - (\tilde{u}, \boldsymbol{a} \cdot \nabla v_h) = \langle f, v_h \rangle \quad \forall v_h \in V_h \tag{3.14}$$

$$(\partial_t \tilde{u}, \tilde{v}) + (\boldsymbol{a} \cdot \nabla u_h, \tilde{v}) + \tau^{-1}(\tilde{u}, \tilde{v}) = 0 \quad \forall \tilde{v} \in V_h^{\perp} \tag{3.15}$$

The important point is that the SGS have been considered time dependent Codina2002 [13]. Their evolution equation can be written as

$$\partial_t \tilde{u} + \tau^{-1} \tilde{u} = -P_h^{\perp}(\boldsymbol{a} \cdot \nabla u_h)$$

If the time derivative of the SGS is neglected, they can be inserted into (3.14) to obtain a closed problem for the finite element component alone which is called Quasi static sub-scale. The full analysis of the resulting formulation can be found in S. Badia and R. Codina2006 [3].

It is interesting to analyze the dissipative structure of problem (3.14)-(3.15). This was done in Principe.2010 [28] in the more complex case of the Navier-Stokes equations. Here we will apply the results of the cited reference to the CDRE.

If, for each fixed t, we take $v_h = u_h$ and $\tilde{v} = \tilde{u}$ in (3.14)-(3.15) it is readily checked that

$$\frac{d}{dt}\|u_h\|^2 + \mathcal{D}_h + \mathcal{T} = \mathcal{P}_h \tag{3.16}$$

$$\frac{d}{dt}\|\tilde{u}\|^2 + \tilde{\mathcal{D}} - \mathcal{T} = \tilde{\mathcal{P}} \tag{3.17}$$

with

$$\mathcal{D}_h = k\|\nabla u_h\|^2 + s\|u_h\|^2 \quad \text{Dissipation of the finite element scale}$$

$$\tilde{\mathcal{D}} = \tau^{-1}\|\tilde{u}\|^2 \quad \text{Dissipation of the SGS}$$

$$\mathcal{T} = (\tilde{u}, \mathcal{L}^* u_h) = -(\tilde{u}, \boldsymbol{a} \cdot \nabla u_h) \quad \text{Energy transfer between scales}$$

These definitions have been introduced thinking of the L^2 norm of the unknown as an energy. In this case, $\mathcal{P}_h$ and $\tilde{\mathcal{P}}$ can be considered the external power applied to the finite element scale and the SGS, respectively. From (3.16)-(3.17), with the definition of the different terms introduced above, we may draw an important conclusion. It is observed that the "energy balance"for the finite element component is the same as for the Galerkin method plus the addition of $\mathcal{T}$, which on average can be shown to be positive. In turn, this additional dissipation is precisely injected with a negative sign in the energy balance equation for the SGS. Therefore, the global energy is conserved, but there is an energy transfer from the "large"scales to the "small"scales. This is the correct dissipative structure

for dissipative systems. In particular, it is crucial for the correct modeling of turbulence.

3.5 Numerical Examples of convection-diffusion using shock capturing techniques

We have chosen two simple numerical test problems to compare numerical efficiency using simple Galerkin method, Galerkin with Algebraic sub-grid scale(ASGS) or Orthogonal sub-scale(OSS) stabilization plus the introduction of shock capturing diffusion, either isotropic (labelled ID what follows), anisotropic(using crosswind dissipation labelled CD) residual based diffusion or orthogonal projection gradient based (labelled OPGB) shock capturing diffusion.

3.5.1 2D homogeneous transient convection-diffusion-reaction problem on a unit square domain

In this section, some tests are conducted to show the numerical performance of normal Galerkin with the orthogonal sub-scale stabilization, hereafter referred to as OSS and also to compare with the algebraic sub-grid scale stabilization method (ASGS) using residual based(ID and CD) and orthogonal projection gradient based(OPGB) shock capturing diffusion which will be added as to capture local oscillation near boundary.

In the first numerical test the convection-diffusion-reaction equation in section (3.2) is numerically solved. In this case, the diffusion coefficient is taken as $k = 10^{-4}$ and force term $f = 10$, reaction coefficient $s = 10$, advection velocity $\boldsymbol{a} = (3, 2)$, boundary condition $\bar{u} = 0$ and shock capturing parameter $C = 0.7$ has been considered. The finite element mesh employed consists of $60 \times 60 Q_1$ elements. The results are shown in the following figure (3.2). The elevation plots of the numerical solution in the first case are shown in figure (3.2) (in this and the following figure the coordinates are measured in grid units). The normal Galerkin method can not reproduce exact solution and it is full of oscillations and instabilities around the whole solution. Comparing both Galerkin plus the ASGS and the OSS stabilization yield very similar solutions in the interior of the computational domain, but the former yields smaller overshoots near the boundaries. This, however, depends on the angle formed by the velocity and the boundary. In particular, in the first case the overshoots near the boundaries parallel to $\boldsymbol{a}$ are almost the same using both methods. The section figure (3.3) clearly indicates that the ASGS and the OSS formulations only yield different results near layers and oscillation near boundaries. Since none of these methods is monotone, both are expected to yield oscillations, being stronger those of the OSS method. However, this needs not to be considered as a bad result for this formulation. Because comparisons should be made combining the ASGS and the OSS methods with a shock or discontinuity-capturing technique.

So using discontinuity capturing techniques it is clearly visible that oscillation has been removed in sharp layers near boundary. Comparing ID, CD using ASGS and OSS with OPGB shock capturing from figure (3.2) it can be observed that both ID and CD shock capturing produces similar results diminishing local oscillation near boundaries, but CD is less overdiffusive than ID. For more details of the convergence criteria using these two methods explained by Codina1993 [8]. Moreover using OPGB with OSS stabilization it exhibits better results near the sharp corners in boundaries than the other two shock capturing methods. It is much smoother near boundaries with slightly overdiffusive behaviour in this occasion.

The shock capturing Orthogonal projection gradient based(OPGB) method for resolution of sharp

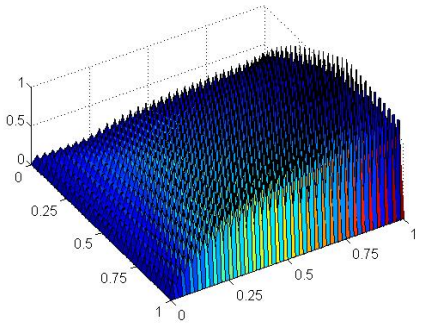

(a) Normal Galerkin

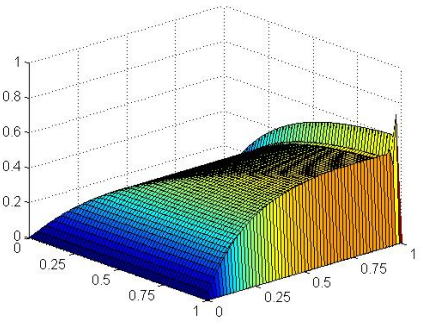

(b) Galerkin+ASGS stabilization

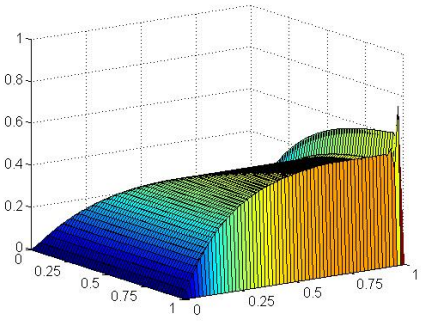

(c) Galerkin+OSS stabilization

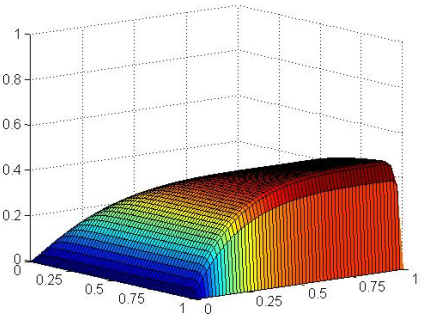

(d) ASGS stabilization with isotropic diffusion(ID)

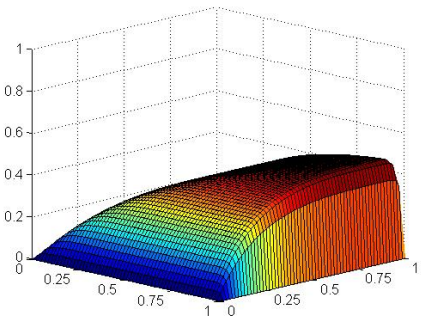

(e) ASGS stabilization with Crosswind dissipation(CD)

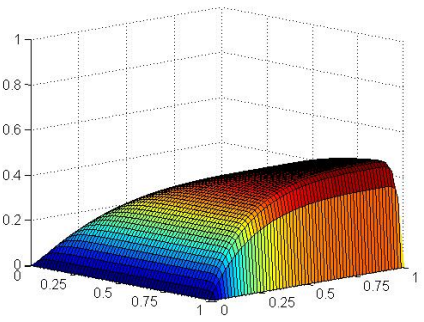

(f) OSS stabilization with Orthogonal projection gradient based(OPGB) dissipation

Fig. 3.2: From top left to right comparison of normal Galerkin and Galerkin formulation with ASGS stabilization. In middle left to right Galerkin formulation with OSS stabilization and using ASGS stabilization with isotropic diffusion(ID). At the bottom from left to right ASGS stabilization with cross wind anisotropic diffusion(CD) shock capturing and Orthogonal projection gradient based(OPGB) shock capturing diffusion using OSS stabilization.

gradients to eliminate local oscillation works well compared to other shock capturing techniques which provides smoother solution near boundaries see section figure(3.4). Comparing with the other two shock capturing methods(ID and CD) in this numerical test it also eliminates local oscillation near the boundary. Here CD shock capturing diffusion is less overdiffusive than the other two shock capturing methods(ID and OPGB). All the shock capturing methods with the combination of a basic stabilization method diminish sharp layers of the numerical solutions.

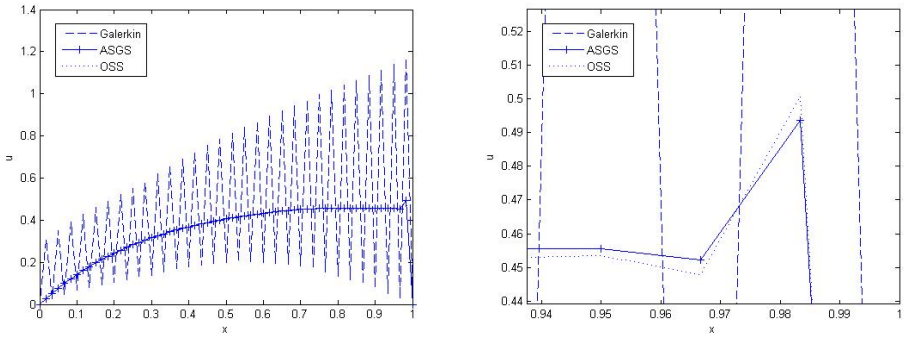

(a) Comparison over full domain (b) Comparison near the boundary

Fig. 3.3: Sectional comparison of normal Galerkin and Galerkin with ASGS and OSS stabilization. Left full domain right zoomed in close to the boundary.

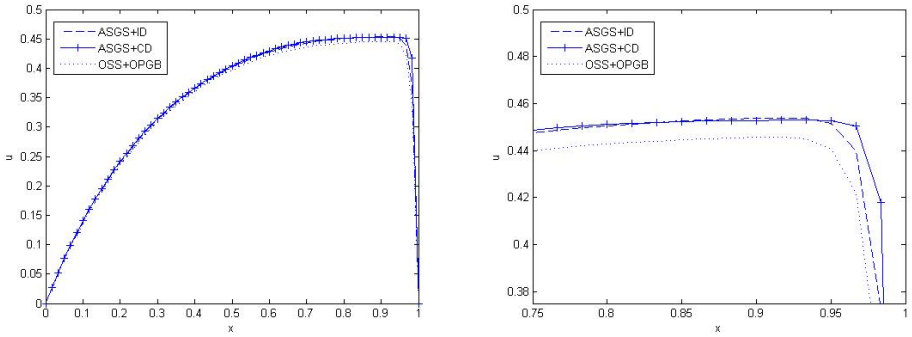

(a) Comparison over full domain (b) Comparison near the boundary

Fig. 3.4: Section figure of comparison of different shock capturing techniques (ID,CD and OPGB). Left full domain right zoomed in close to the boundary.

3.5.2 Solid body rotation

This numerical test was followed from Kuzmin2010 [30]. Solid body rotation illustrates the ability of a numerical scheme to transport initial data without distortion. Consider the linear convection equation.

$$\partial_t u + \nabla \cdot (\boldsymbol{v} u) = 0 \quad \text{in} \quad \Omega = (-0.5, 1.5) \times (-0.5, 1.5) \tag{3.18}$$

which is a hyperbolic equation and where the incompressible velocity field

$$\boldsymbol{v}(x, y) = (0.5 - y, x - 0.5) \tag{3.19}$$

corresponds to a counterclockwise rotation about the center of the square domain Ω. Homogeneous Dirichlet boundary conditions are prescribed at the inlets. The exact solution to (3.18)-(3.19) depends solely on the initial state u_0 and reproduces it exactly after each full revolution without any local oscillation in the sharp corners. Hence, the challenge of this test is to preserve the shape of u_0 as accurately as possible. For this numerical problem we use Galerkin method without stabilization parameter, Algebraic sub-grid scale(ASGS) and Orthogonal sub-scale(OSS) stabilization with isotropic(ID), anisotropic or crosswind dissipation(CD) and orthogonal projection gradient based (OPGB) shock capturing diffusion. Here the Crank Nicholson scheme has been used for the temporal

discretization.

We consider a cylinder and a cone of an initial geometry depicted in (Fig. 3.5).
Initially, the geometry of the body is given by a function $G(x, y)$ defined within the circle

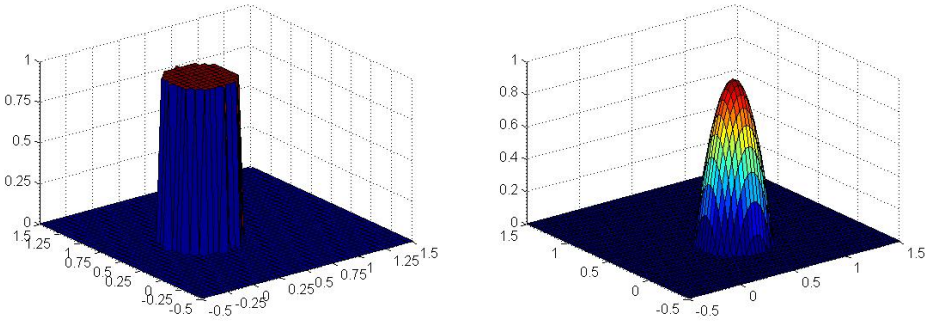

(a) Initial geometry of the cylinder (b) Initial geometry of the cone

Fig. 3.5: Initial geometry of the cylinder and cone at t=0.

$$r(x, y) = \frac{1}{r_0}\sqrt{(x - x_0)^2 + (y - y_0)^2} \leqslant 1$$

of radius $r_0 = 0.3$ centered at a certain point with Cartesian coordinates (x_0, y_0).
For the rotating cylinder and cone, the reference point is $(x_0, y_0) = (0.5, 0.25)$ and for the cylinder

$$G(x, y) = \begin{cases} 1 & \text{if } r \leqslant 1, \\ 0 & \text{else } 0 \end{cases}$$

and for the cone

$$G(x, y) = 1 - r(x, y)$$

Figure (3.6) displays the results produced by the Crank-Nicolson time integration scheme using pure Galerkin finite element method without stabilization parameter and Galerkin method with Algebric subgrid scale(ASGS) and Orthogonal sub-scale(OSS) stabilization method of this rotating cylinder after one full revolution $t = 2\pi$. These numerical solutions were computed on a uniform mesh of 60×60 bilinear elements, $h = 0.02357$ and $\Delta t = \frac{2\pi}{120}$.

From the figure (3.6) it is seen that without stabilization the standard Galerkin method cannot resolute the exact solution and shows oscillations around the whole solution. Boundary layers are present in the solution due to the convective character of the equation and homogeneous Dirichlet boundary conditions. For this reason in the Galerkin formulation it appears full of instabilities in the solution. Comparing to Galerkin solution using stabilized formulation ASGS and OSS method the solution can eliminate the oscillation around the rotating cylinder and the boundary but still local oscillation remains in the sharp corners of the cylinder. ASGS and OSS alleviate oscillation and provide very similar results with the improvement of the numerical solution.

Using ASGS with the isotropic diffusion(ID) and crosswind dissipation(CD) (see figure (3.7)) it is seen that both shock capturing techniques eliminates the local oscillation near sharp layers and corners of the rotating cylinder. Both ID and CD method generate similar results in this occasion with ASGS stabilization. In the case of OPGB shock capturing techniques with OSS stabilization it

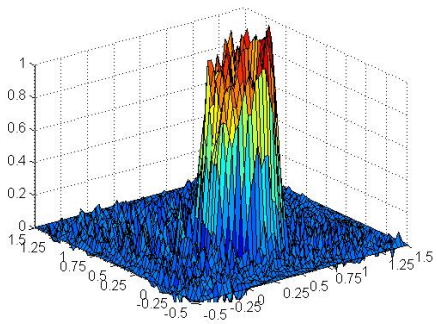

(a) Simple Galerkin elevation plot

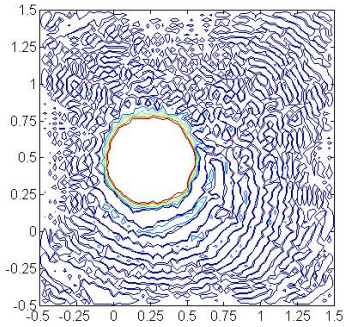

(b) Simple Galerkin contour plot

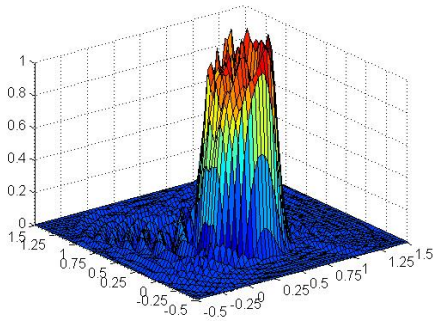

(c) Galerkin+ASGS stabilization evevation plot

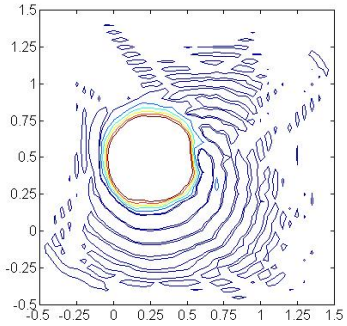

(d) Galerkin+ASGS stabilization contour plot

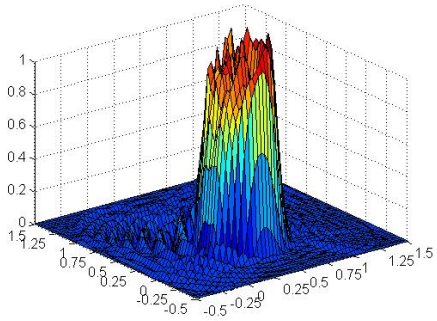

(e) Galerkin+OSS stabilization evevation plot

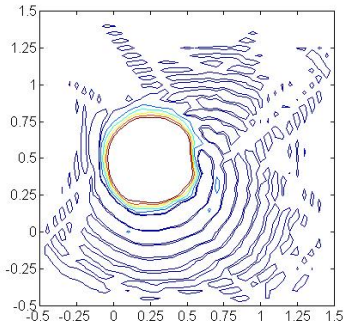

(f) Galerkin+OSS stabilization contour plot

Fig. 3.6: Results of the rotating cylinder problem from top to bottom Galerkin without stabilization parameter, middle Galerkin with ASGS stabilization and bottom Galerkin with OSS stabilization method. Left(elevation plot) and right(contour plot).

is less overdiffusive comparing to other methods.

The same numerical results can be found in the rotating cone case from figure (3.8). The Galerkin method cannot reproduce the exact solution in the highly convective dominated case and it is full of spurious oscillation around the cone. Galerkin method with ASGS and OSS stabilization reproduce better solutions than simple Galerkin method with less oscillation but cannot fully remove spurious oscillations around the sharp corners of the cone where gradient of sharp layers are present. Local oscillation free solutions can be obtained introducing shock capturing techniques.

From figure (3.9) it can be explained that local oscillations usually observed in the previous figure (3.8) with stabilization are completely removed introducing shock capturing techniques. Both

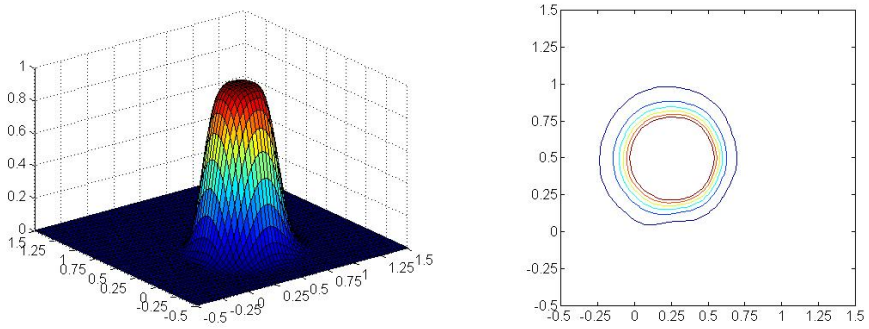

(a) ASGS+ID elevation plot (b) ASGS+ID contour plot

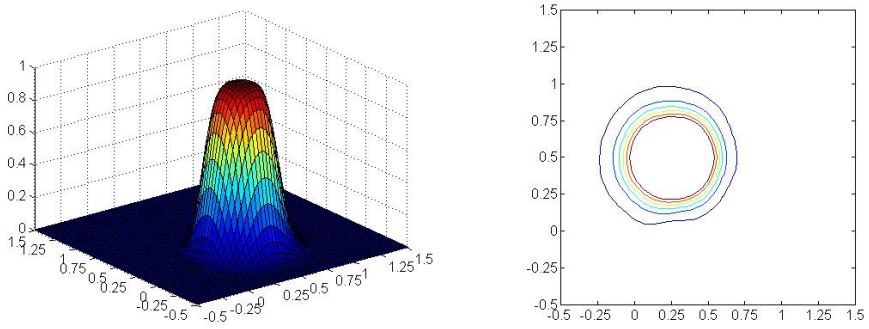

(c) ASGS+CD evevation plot (d) ASGS+CD contour plot

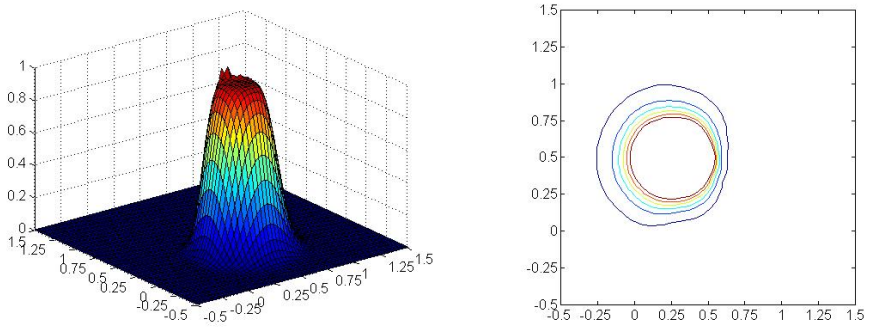

(e) OSS+OPGB evevation plot (f) OSS+OPGB contour plot

Fig. 3.7: From top to bottom rotating cylinder numerical results ASGS with isotropic diffusion(ID), ASGS with Anisotropic crosswind dissipation(CD) and OSS method using Orthogonal projection gradient based(OPGB) shock capturing technique. Left(elevation plot) and right(contour plot).

ASGS stabilization with ID and CD shock capturing diffusion provide smooth solution and good resolution in sharp layers and corners. Similar results can be found with the OSS stabilization using orthogonal projection gradient based(OPGB) shock capturing diffusion increasing the amount of numerical dissipation in the neighbourhood layers.

Using orthogonal projection gradient based(OPGB) shock capturing technique with OSS stabilization result is less over diffusive behaviour than the other shock capturing techniques comparing the sections figure (3.10). Both ID and CD shock capturing techniques with ASGS stabilization exhibits similar profile of the cylinder and cone after one full revolution but more diffusive than OPGB. The shock capturing parameter $C = 0.1$ has been used for calculating the artificial diffusion.

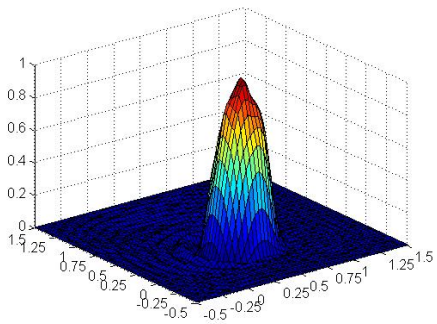

(a) Simple Galerkin elevation plot

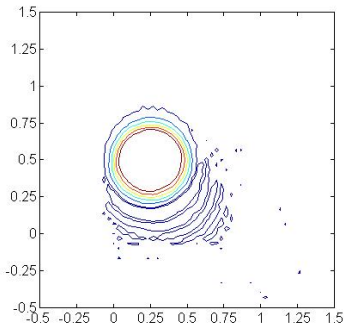

(b) Simple Galerkin contour plot

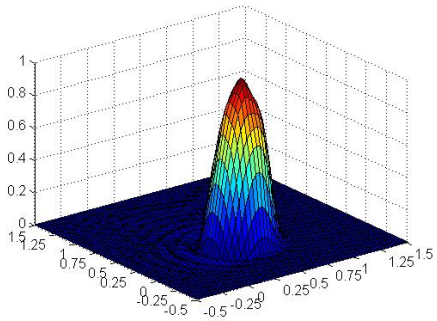

(c) Galerkin+ASGS stabilization evevation plot

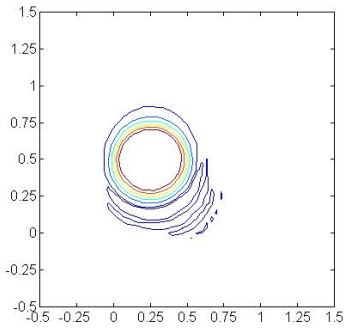

(d) Galerkin+ASGS stabilization contour plot

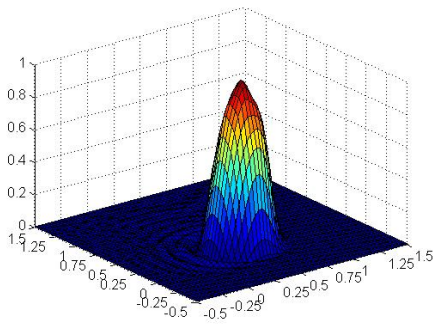

(e) Galerkin+OSS stabilization evevation plot

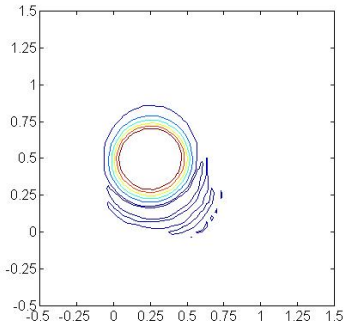

(f) Galerkin+OSS stabilization contour plot

Fig. 3.8: Results of the rotating cone problem from top to bottom Galerkin without stabilization parameter, middle Galerkin with ASGS stabilization method and bottom Galerkin with OSS stabilization method. Left(elevation plot) and right(contour plot).

This OPGB discontinuity capturing diffusion is added isotropically. Every shock capturing produce smooth solution eliminating oscillation near sharp layers in the cylinder and cone. So using shock capturing diffusion eliminates local oscillation about abrupt layers of the solution and prevents global failure of the numerical solutions for the highly nonlinear convection dominated problem.

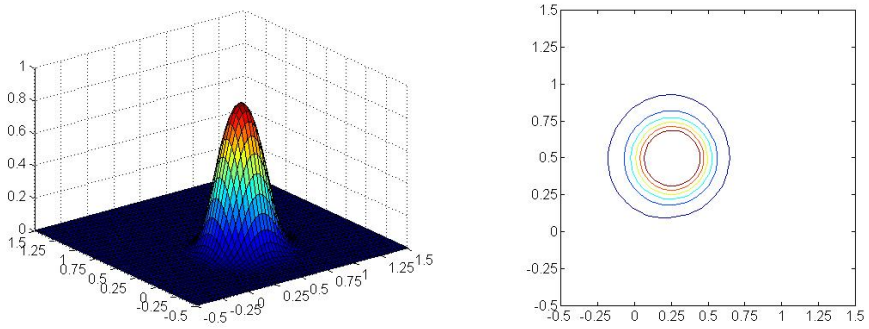

(a) ASGS+ID elevation plot (b) ASGS+ID contour plot

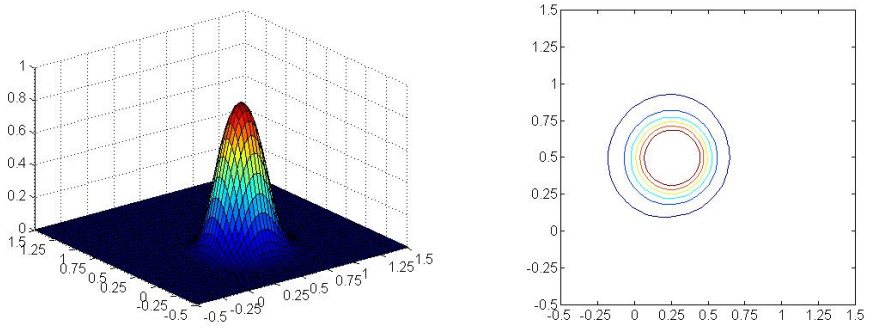

(c) ASGS+CD evevation plot (d) ASGS+CD contour plot

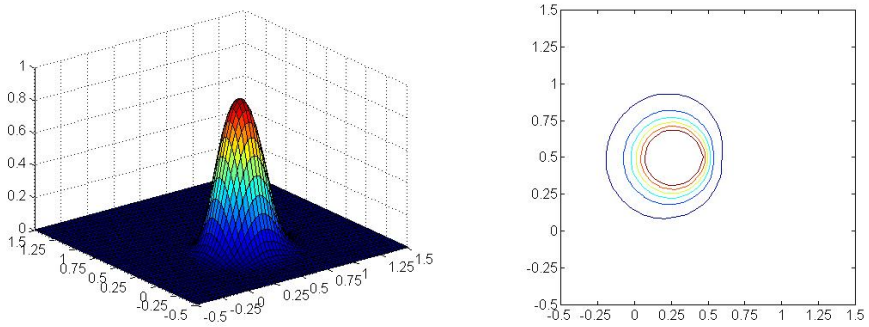

(e) OSS+OPGB evevation plot (f) OSS+OPGB contour plot

Fig. 3.9: From top to bottom rotating cone numerical results ASGS with isotropic diffusion(ID), ASGS with Anisotropic crosswind dissipation(CD) and OSS method using Orthogonal projection gradient based(OPGB) shock capturing technique. Left(elevation plot) and right(contour plot).

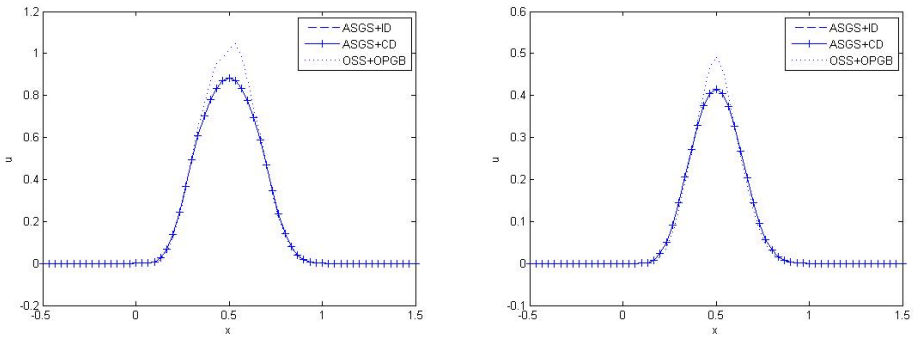

(a) Shock capturing comparison for cylinder (b) Shock capturing comparison for cone

Fig. 3.10: Section comparison using ID,CD and OPGB shock capturing techniques with different stabilization methods after full revolution of the cylinder(Left) and cone(Right).

Chapter 4

Numerical approximation of thermally coupled incompressible flows

4.1 Finite Element Approximation

In this chapter we propose a variational multiscale finite element approximation of thermally coupled flows. We consider the thermal coupling in the context of the Boussinesq approximation coupling the incompressible Navier Stokes equation and heat equation. The main feature of the formulation in contrast to other stabilized methods is that we consider the subscales as time dependent. They are solution of a differential equation in time that needs to be integrated. Likewise, we keep the effect of the subscales both in the nonlinear convective terms of the momentum and temperature equations and, if required, the coupling between them. Here in this chapter we discuss about temporal discretization, conservation of linear momentum and heat and discuss the possibility a of modeling turbulence using Large Eddy Simulation(LES).

4.1.1 Variational Formulation

To define functional setting, let $H^1(\Omega)$ be the space of functions such that they and their first derivatives belong to $L^2(\Omega)$ (that is, they are square integrable), and let $H_0^1(\Omega)$ be the subspace of functions in $H^1(\Omega)$ vanishing on the boundary. Let also $\boldsymbol{V}_{st} = H_0^1(\Omega)^d$, $Q_{st} = L^2(\Omega)/\mathbb{R}$, $\Psi_{st} = H_0^1(\Omega)$ and define $\boldsymbol{V} = L^2(0,T;\boldsymbol{V}_{st})$, $Q = L^1(0,T;Q_{st})$ (for example) and $\Psi = L^2(0,T;\Psi_{st})$, where $L^p(0,T;X)$ stands of the space of functions such that their X norm in the spatial argument is an $L^p(0,T)$ function in time, that is, its p-th power is integrable if $1 \leqslant p < \infty$ or bounded if $p = \infty$.

The weak form of the problem consists in finding $(\boldsymbol{u}, p, \vartheta) \in \boldsymbol{V} \times Q \times \Psi$ such that:

$$(\partial_t \boldsymbol{u}, \boldsymbol{v}) + \langle \boldsymbol{u} \cdot \nabla \boldsymbol{u}, \boldsymbol{v} \rangle + \nu\,(\nabla \boldsymbol{u}, \nabla \boldsymbol{v}) - (p, \nabla \cdot \boldsymbol{v}) + \alpha\,(\boldsymbol{g}\vartheta, \boldsymbol{v}) = \langle \boldsymbol{f}, \boldsymbol{v} \rangle + \alpha\,(\boldsymbol{g}\vartheta_0, \boldsymbol{v}) \tag{4.1}$$

$$(q, \nabla \cdot \boldsymbol{u}) = 0, \tag{4.2}$$

$$(\partial_t \vartheta, \psi) + \langle \boldsymbol{u} \cdot \nabla \vartheta, \psi \rangle + \kappa\,(\nabla \vartheta, \nabla \psi) = \langle Q, \psi \rangle, \tag{4.3}$$

for all $(\boldsymbol{v}, q, \psi) \in \boldsymbol{V}_{st} \times Q_{st} \times \Psi_{st}$, where $(\cdot, \cdot)$ denotes the $L^2(\Omega)$ inner product and $\langle f, g \rangle := \int_\Omega fg$ whenever functions f and g are such that the integral is well defined.

The dimensionless numbers relevent in this problem are:

$$Re := \frac{LU}{\nu}, \qquad \text{Reynolds number} \tag{4.4}$$

$$Pe := \frac{LU}{\kappa}, \qquad \text{Peclet Number} \tag{4.5}$$

$$Pr := \frac{\nu}{\kappa}, \qquad \text{Prandl Number} \tag{4.6}$$

$$Ra := \frac{\alpha|\boldsymbol{g}|L^3\delta\vartheta}{\nu\kappa}, \qquad \text{Rayleigh Number} \tag{4.7}$$

where L is a characteristic length, U is a characteristic velocity and $\delta\theta$ is a characteristic temperature difference, usually computed from temperature boundary values when these are not zero. When U cannot be determined by the boundary conditions, for example because zero velocities are prescribed, $U = \nu/L$ can be taken, which corresponds to choose $Re = 1$ and that gives $Pe = Pr$.

4.1.2 Scale Splitting

Let us consider a finite element partition $\{K\}$ with n_e elements of the computational domain Ω, from which we can construct finite element spaces for velocity, pressure and temperature in the usual manner. We will assume that they are all built from continuous piecewise polynomials of the same degree k. The basic idea of the multiscale approach we will follow (see Hughes et al.1998 [49]) is to split the continuous unknowns as:

$$\boldsymbol{u} = \boldsymbol{u}_h + \tilde{\boldsymbol{u}} \tag{4.8}$$

$$p = p_h + \tilde{p} \tag{4.9}$$

$$\vartheta = \vartheta_h + \tilde{\vartheta} \tag{4.10}$$

where the components with subscript h belong to the corresponding finite element spaces. The components with a tilde belong to any space such that its direct sum with the finite element space yields the functional space where the unknown is sought. For the moment, we leave it undefined. These additional components are what we will call subscales. Each particular variational multiscale method will depend on the way the subscales are approximated. Our main focus in this work is to explain the consequences of considering these subscales time dependent, and therefore requiring to be integrated in time. Likewise, we will keep the previous decompositions $(4.8 - 4.10)$ in all the terms of the variational equations of the problem. As we shall see, this has important consequences in the modeling of thermally coupled turbulent flows. The only approximation we will make for the moment is to assume that the subscales vanish on the interelement boundaries, $\partial\Omega_e$. This happens for example if one assumes that their Fourier modes correspond to high wave numbers, as it is explained in Codina 2002 [13], but can be relaxed using the approach proposed in Codina et al.2009 [39].

From the previous splitting two sets of equations can be obtained. The first is the projection of the original equations onto the finite element spaces of velocity, pressure and temperature. On the other hand, the equations for the subscales are obtained by projecting onto their corresponding spaces, that is, by taking the test function $\tilde{\boldsymbol{v}}$ in the space of subscales instead of in the finite element space. If $\tilde{P}$ denotes the projection onto any of the subscale spaces (for velocity, pressure or temperature), these equations are:

$$\tilde{P}[\partial_t\tilde{\boldsymbol{u}} + (\boldsymbol{u}_h + \tilde{\boldsymbol{u}}) \cdot \nabla\tilde{\boldsymbol{u}} - \nu\Delta\tilde{\boldsymbol{u}} + \nabla\tilde{p} + \alpha\boldsymbol{g}\tilde{\vartheta}] = \tilde{P}\left(\boldsymbol{R}_u\right) \tag{4.11}$$

$$\tilde{P}\left(\nabla \cdot \tilde{\boldsymbol{u}}\right) = \tilde{P}\left(R_p\right) \tag{4.12}$$

$$\tilde{P}[\partial_t\tilde{\vartheta} + (\boldsymbol{u}_h + \tilde{\boldsymbol{u}}) \cdot \nabla\tilde{\vartheta} - \kappa\Delta\tilde{\vartheta}] = \tilde{P}\,(R_\vartheta) \tag{4.13}$$

Where:

$$\boldsymbol{R}_u = \boldsymbol{f} + \alpha\boldsymbol{g}\vartheta_0 - [\partial_t\boldsymbol{u}_h + (\boldsymbol{u}_h + \tilde{\boldsymbol{u}}) \cdot \nabla\boldsymbol{u}_h - \nu\Delta_h\boldsymbol{u}_h + \nabla p_h + \alpha\boldsymbol{g}\vartheta_h],$$

$$R_p = -\nabla \cdot \boldsymbol{u}_h,$$

$$R_\vartheta = Q - [\partial_t\vartheta_h + (\boldsymbol{u}_h + \tilde{\boldsymbol{u}}) \cdot \nabla\vartheta_h - \kappa\Delta_h\vartheta_h],$$

are the residuals of the finite element unknowns in the momentum, continuity and heat equation, respectively. Equations (4.11 - 4.13) need to be solved within each element and as we have assumed, considering homogeneous velocity and temperature Dirichlet boundary conditions.

The general procedure to approximate the subscales in problems (4.11 - 4.13) and in particular, of the spatial differential operators applied to the subgrid scales has been explained in details in Codina et al. 2010 [41].

4.1.3 Approximation of the subscales: application to thermally coupled flows

It is not our purpose here to discuss how to approximate (4.11 - 4.13) which, in fact, is the essence of the different stabilized finite element methods that can be found in the literature. We will adopt a simple approximation that can be found, for example, in Codina 2002 [13] and references therein. Our main concern, as in the reference just mentioned, is to keep *the time dependence of the subscales, as well their nonlinear effects*. When their time derivative is neglected, we will call them *quasi-static subscale*, whereas otherwise we will call them *dynamic subscales*.

Let us introduce the stabilization parameters τ_1, τ_2 and τ_3, computed as:

$$\tau_1 = [(c_1\frac{\nu}{h^2})^2 + (c_2\frac{|\boldsymbol{u}_h + \tilde{\boldsymbol{u}}|}{h})^2]^{-1/2}, \tag{4.14}$$

$$\tau_2 = \frac{h^2}{c_1\tau_1}, \tag{4.15}$$

$$\tau_3 = [(c_1\frac{\kappa}{h^2})^2 + (c_2\frac{|\boldsymbol{u}_h + \tilde{\boldsymbol{u}}|}{h})^2]^{-1/2}, \tag{4.16}$$

Where h is the element size and c_1 and c_2 are algorithmic constants(we have adopted $c_1 = 4$ and $c_2 = 2$ in the numerical experiments).

For the thermally coupled flows, we propose to compute the subscales within each element of the finite element partition as solution to

$$\partial_t\tilde{\boldsymbol{u}} + \frac{1}{\tau_1}\tilde{\boldsymbol{u}} = \tilde{P}(\boldsymbol{R}_u), \tag{4.17}$$

$$\frac{1}{\tau_1}\tilde{p} = \tilde{P}(R_p + \tau_1\partial_t R_p), \tag{4.18}$$

$$\partial_t\tilde{\vartheta} + \frac{1}{\tau_3}\tilde{\vartheta} = \tilde{P}(R_\vartheta), \tag{4.19}$$

The approximation adopted for the subscales could certainly be improved, for example by trying to relax the assumption that they vanish on the interelement boundaries or by trying to model the coupling between the three equations in play (momentum, continuity and heat) which has been followed

in Principe2009 [38]. However, our interest here is only to analyze the effect of considering the subscales time dependent and taking into account their contribution in the nonlinear terms. In particular, it is important to remark that (4.17) is nonlinear, both because the velocity subscale contributes to the advection velocity and because the stabilization parameter τ_1 depends on velocity subscale as equation (4.19) and the stabilization parameter τ_3. Likewise, (4.17) depends on the temperature subscale, and therefore the velocity-temperature coupling is naturally accounted for.

4.1.4 Final approximate problem in space

Substituting Equations (4.8-4.10) into Equations (2.1-2.3), taking the test functions in the corresponding finite element spaces and integrating some terms by parts, and using the fact that $\boldsymbol{u} = \boldsymbol{u}_h + \tilde{\boldsymbol{u}}$ is divergence free, it is found that:

$$\begin{aligned}(\partial_t \boldsymbol{u}_h, \boldsymbol{v}_h) + (\boldsymbol{u}_h \cdot \nabla \boldsymbol{u}_h, \boldsymbol{v}_h) + \nu(\nabla \boldsymbol{u}_h, \nabla \boldsymbol{v}_h) \\ -(p_h, \nabla \cdot \boldsymbol{v}_h) + \alpha(\boldsymbol{g}\vartheta_h, \boldsymbol{v}_h) - \langle \tilde{\boldsymbol{u}}, \nu \Delta_h \boldsymbol{v}_h + \boldsymbol{u}_h \cdot \nabla \boldsymbol{v}_h \rangle \\ +(\partial_t \tilde{\boldsymbol{u}}, \boldsymbol{v}_h) + \langle \tilde{\boldsymbol{u}} \cdot \nabla \boldsymbol{u}_h, \boldsymbol{v}_h \rangle - \langle \tilde{\boldsymbol{u}}, \tilde{\boldsymbol{u}} \cdot \nabla \boldsymbol{v}_h \rangle - (\tilde{p}, \nabla \cdot \boldsymbol{v}_h) \\ +\alpha(\boldsymbol{g}\tilde{\vartheta}, \boldsymbol{v}_h) = \langle \boldsymbol{f}, \boldsymbol{v}_h \rangle + \alpha(\boldsymbol{g}\vartheta_0, \boldsymbol{v}_h),\end{aligned} \tag{4.20}$$

$$(q_h, \nabla \cdot \boldsymbol{u}_h) - (\tilde{\boldsymbol{u}}, \nabla q_h) = 0, \tag{4.21}$$

$$\begin{aligned}(\partial_t \vartheta_h, \psi_h) + \langle \boldsymbol{u}_h \cdot \nabla \vartheta_h, \psi_h \rangle + \kappa(\nabla \vartheta_h, \nabla \psi_h) \\ -\langle \tilde{\vartheta}, \kappa \Delta_h \psi_h + \boldsymbol{u}_h \cdot \nabla \psi_h \rangle + (\partial_t \tilde{\vartheta}, \psi_h) + \langle \tilde{\boldsymbol{u}} \cdot \nabla \vartheta_h, \psi_h \rangle \\ -\langle \tilde{\vartheta}, \tilde{\boldsymbol{u}} \cdot \nabla \psi_h \rangle = \langle Q, \psi_h \rangle,\end{aligned} \tag{4.22}$$

which must hold for all test functions $(\boldsymbol{v}_h, q_h, \psi_h) \in (\boldsymbol{V}_h, Q_h, \Psi_h)$. The subindex h in the Laplacian denotes that it is evaluated elementwise. The subscales in these equations are obtained from Equations (4.17-4.19). The first approximation involved in the previous equations is to assume that the subscales vanish at the interelement boundaries. The final numerical scheme is obtained by approximating these subscales in the element interiors, in our case by means of Equations (4.17-4.19).

These equations however still require the definition of the projections $\tilde{P}$. Classical stabilized finite element methods correspond to taking $\tilde{P} = I$ (identity) when applied to the corresponding finite element residual(Algebraic sub-grid scale). Our proposal however is to take $\tilde{P} = P_h^{\perp} = I - P_h$, where P_h is the L^2 projection onto the finite element space(see Codina2002 [13] and, for an analysis of the method for a stationary and linearized problem Codina2008 [11]). This leads to what we call orthogonal sub-scale stabilization (OSS). When this is used in Equations (4.20-4.22) one gets the following equations:

$$\begin{aligned}(\partial_t \boldsymbol{u}_h, \boldsymbol{v}_h) + (\boldsymbol{u}_h \cdot \nabla \boldsymbol{u}_h, \boldsymbol{v}_h) + \nu(\nabla \boldsymbol{u}_h, \nabla \boldsymbol{v}_h) \\ -(p_h, \nabla \cdot \boldsymbol{v}_h) + \alpha(\boldsymbol{g}\vartheta_h, \boldsymbol{v}_h) \\ -\langle \tilde{\boldsymbol{u}}, \nu \Delta_h \boldsymbol{v}_h + \boldsymbol{u}_h \cdot \nabla \boldsymbol{v}_h \rangle + \langle \tilde{\boldsymbol{u}} \cdot \nabla \boldsymbol{u}_h, \boldsymbol{v}_h \rangle \\ -\langle \tilde{\boldsymbol{u}}, \tilde{\boldsymbol{u}} \cdot \nabla \boldsymbol{v}_h \rangle - (\tilde{p}, \nabla \cdot \boldsymbol{v}_h) = \langle \boldsymbol{f}, \boldsymbol{v}_h \rangle + \alpha(\boldsymbol{g}\vartheta_0, \boldsymbol{v}_h),\end{aligned} \tag{4.23}$$

$$(q_h, \nabla \cdot \boldsymbol{u}_h) - (\tilde{\boldsymbol{u}}, \nabla q_h) = 0, \tag{4.24}$$

$$
\begin{aligned}
(\partial_t \vartheta_h, \psi_h) + \langle \boldsymbol{u}_h \cdot \nabla \vartheta_h, \psi_h \rangle + \kappa(\nabla \vartheta_h, \nabla \psi_h) & \\
- \langle \tilde{\vartheta}, \kappa \Delta_h \psi_h + \boldsymbol{u}_h \cdot \nabla \psi_h \rangle + \langle \tilde{\boldsymbol{u}} \cdot \nabla \vartheta_h, \psi_h \rangle & \\
- \langle \tilde{\vartheta}, \tilde{\boldsymbol{u}} \cdot \nabla \psi_h \rangle = \langle Q, \psi_h \rangle, &
\end{aligned}
\tag{4.25}
$$

Note that $(\partial_t \tilde{\boldsymbol{u}}, \boldsymbol{v}_h)$ and $\alpha(\boldsymbol{g}\tilde{\vartheta}, \boldsymbol{v}_h)$ vanish in equation (4.20) and $(\partial_t \tilde{\vartheta}, \psi_h)$ vanishes in equation (4.22) because of the choice $\tilde{P} = P_h^{\perp}$. Any time discretization can now be applied to obtain a fully discrete problem.

4.2 Temporal Discretization

Any finite difference scheme can now be applied to discretize in time both equations (4.20-4.22) and equations (4.23-4.25). Obviously, space-time finite element discretizations are also possible. In order to make the exposition concise, we will restrict our attention to the trapezoidal rule.

Let δt be the time step size of a uniform partition of the time interval $[0, T]$, $0 = t^0 < t^1 < t < ... < t^N = T$. Functions approximated at time t^n will be identified with the superscript n. For a generic function f, we will use the notation $\delta f^n := f^{n+1} - f^n$, $\delta_t f^n = \delta f^n / \delta t$, $f^{n+\theta} = \theta f^{n+1} + (1-\theta) f^n, 0 \leqslant \theta \leqslant 1$.

The time discretization of (4.20-4.22) is standard and does not need any further explanation. Given $\boldsymbol{u}_h^n$, ϑ_h^n, $\tilde{\boldsymbol{u}}^n$ and $\tilde{\vartheta}^n$, it consists of solving the problem

$$
\begin{aligned}
(\delta_t \boldsymbol{u}_h^n, \boldsymbol{v}_h) + (\boldsymbol{u}_h^{n+\theta} \cdot \nabla \boldsymbol{u}_h^{n+\theta}, \boldsymbol{v}_h) + \nu(\nabla \boldsymbol{u}_h^{n+\theta}, \nabla \boldsymbol{v}_h) & \\
- (p_h^{n+1}, \nabla \cdot \boldsymbol{v}_h) + \alpha(\boldsymbol{g}\vartheta_h^{n+\theta}, \boldsymbol{v}_h) - \langle \tilde{\boldsymbol{u}}^{n+\theta}, \nu \Delta_h \boldsymbol{v}_h + \boldsymbol{u}_h^{n+\theta} \cdot \nabla \boldsymbol{v}_h \rangle & \\
+ (\delta_t \tilde{\boldsymbol{u}}^n, \boldsymbol{v}_h) + \langle \tilde{\boldsymbol{u}}^{n+\theta} \cdot \nabla \boldsymbol{u}_h^{n+\theta}, \boldsymbol{v}_h \rangle - \langle \tilde{\boldsymbol{u}}^{n+\theta}, \tilde{\boldsymbol{u}}^{n+\theta} \nabla \cdot \boldsymbol{v}_h \rangle & \\
- (\tilde{p}^{n+1}, \nabla \cdot \boldsymbol{v}_h) + \alpha(\boldsymbol{g}\tilde{\theta}^{n+\theta}, \boldsymbol{v}_h) = \langle \boldsymbol{f}, \boldsymbol{v}_h \rangle + \alpha(\boldsymbol{g}\vartheta_0, \boldsymbol{v}_h), &
\end{aligned}
\tag{4.26}
$$

$$
(q_h, \nabla \cdot \boldsymbol{u}_h^{n+\theta}) - (\tilde{\boldsymbol{u}}^{n+\theta}, \nabla q_h) = 0, \tag{4.27}
$$

$$
\begin{aligned}
(\delta_t {\vartheta_h}^n, \psi_h) + \langle \boldsymbol{u}_h^{n+\theta} \cdot \nabla \vartheta_h^{n+\theta}, \psi_h \rangle + \kappa(\nabla \vartheta_h^{n+\theta}, \nabla \psi_h) & \\
- \langle \tilde{\vartheta}^{n+\theta}, \kappa \Delta_h \psi_h + \boldsymbol{u}_h^{n+\theta} \cdot \nabla \psi_h \rangle + (\delta_t \tilde{\vartheta}^n, \psi_h) + \langle \tilde{\boldsymbol{u}}^{n+\theta} \cdot \nabla \vartheta_h^{n+\theta}, \psi_h \rangle & \\
- \langle \tilde{\vartheta}^{n+\theta}, \tilde{\boldsymbol{u}}^{n+\theta} \cdot \nabla \psi_h \rangle = \langle Q, \psi_h \rangle, &
\end{aligned}
\tag{4.28}
$$

which must hold for all test functions $(\boldsymbol{v}_h, q_h, \psi_h) \in (\boldsymbol{V}_h, Q_h, \Psi_h)$. Note that the pressure is considered approximated at time $n+1$. This avoids the need to deal with the pressure at a previous time step and does not modify the velocity approximation. As it is well known, the scheme is expected to be of second order if $\theta = \frac{1}{2}$ and of first order otherwise. The equations for the subscales are:

$$
\delta_t \tilde{\boldsymbol{u}}^n + \frac{1}{\tau_1^{n+\theta}} \tilde{\boldsymbol{u}}^{n+\theta} = \tilde{P}(\boldsymbol{R}_u^{n+\theta}), \tag{4.29}
$$

$$
\frac{1}{\tau_2^{n+1}} \tilde{p}^{n+1} = \tilde{P}(R_p^{n+1} + \tau_1^{n+1} \delta_t R_p^n), \tag{4.30}
$$

$$
\delta_t \tilde{\vartheta}^n + \frac{1}{\tau_3^{n+\theta}} \tilde{\vartheta}^{n+\theta} = \tilde{P}(R_\vartheta^{n+\theta}), \tag{4.31}
$$

However, we will consider two additional options. The first is that the time integration for the subscales could be less accurate than for the finite element equations(4.20 - 4.22) and still keep the same order of accuracy in time of the finite element solution. The formal idea to justify this is the following. From the expression of the stabilization parameters τ_1 and τ_3 in (4.14) and (4.16), respectively, it follows that they behave as the critical time steps of an explicit integration in time of the momentum and the heat equation Codina et al.2002 [13]. Therefore, we may assume that they are of order $\mathcal{O}(\delta t)$. From (4.29) it follows that $\mathcal{O}(1)\delta\tilde{\boldsymbol{u}}^{n+1} + \tilde{\boldsymbol{u}}^{n+1} = \mathcal{O}(\delta t)\tilde{P}(\boldsymbol{R}_u^{n+\theta})$, and thus we may conclude that $\tilde{\boldsymbol{u}}^{n+1} = \mathcal{O}(\delta t)\tilde{P}(\boldsymbol{R}_u^{n+1})$. If the residual of the finite element component is bounded, $|\tilde{\boldsymbol{u}}^{n+1} - \tilde{\boldsymbol{u}}^{n}| = \mathcal{O}(\delta t^2)$, and therefore evaluating the subscale at $n+1$, for example, in (4.26) instead of at $n+\theta$ introduces an error of order δt^2, which is the optimal error that can be reached with the trapezoidal rule (for $\theta = 1/2$). The same comments apply to (4.31) for temperature subscale.

Considering the subscale equations integrated to first order and the finite element equations to second (or higher) is not particularly relevant in the case of the trapezoidal rule. However, if, for example, the second order backward-differencing (BDF) scheme is used, a first order integration of the equation for the subscales avoids the need to store them in two previous time steps. This storage is the most important cost of integrating the subscales in time. Another aspect to take into account is that the subscale approximation is not smooth, since the residual of the finite element components will be discontinuous across interelement boundaries. Thus, it seems reasonable to use a scheme as dissipative as possible to integrate the subscales in time. See further comments about this point can be found in Principe2009 [38].

A first order time integration for the subscales is straightforward. Equations (4.29) and (4.31) have to be replaced by their counterparts for $\theta = 1$. A third and final possibility that can be considered to integrate (4.17 - 4.19) in time is a combination of exact integration and approximation of the stabilization parameters and residuals at $t^{n+\theta}$

$$\partial_t\tilde{\boldsymbol{u}} + \frac{1}{\tau_1^{n+\theta}}\tilde{\boldsymbol{u}} = \tilde{P}(\boldsymbol{R}_u^{n+\theta}),$$

$$\partial_t\tilde{\vartheta} + \frac{1}{\tau_3^{n+\theta}}\tilde{\vartheta} = \tilde{P}(R_\vartheta^{n+\theta}),$$

This can be integrated exactly, yielding

$$\tilde{\boldsymbol{u}}^{n+1} = \tilde{\boldsymbol{u}}^{n} - \tau_1^{n+\theta}\tilde{P}(\boldsymbol{R}_u^{n+\theta})\exp(-\frac{\delta t}{\tau_1^{n+\theta}}) + \tau_1^{n+\theta}\tilde{P}(\boldsymbol{R}_u^{n+\theta}) \tag{4.32}$$

$$\tilde{\vartheta}^{n+1} = \tilde{\vartheta}^{n} - \tau_3^{n+\theta}\tilde{P}(R_\vartheta^{n+\theta})\exp(-\frac{\delta t}{\tau_3^{n+\theta}}) + \tau_3^{n+\theta}\tilde{P}(R_\vartheta^{n+\theta}) \tag{4.33}$$

4.3 Main Features of the formulation

The first and most important point to be considered is the effect of considering the subscales dynamic, and therefore to deal with their time variation. Some of these properties are:

1. The effect of the time integration is now clear. Certainly, when the time discretization is introduced the effective stabilization parameters have to be modified (as it is done for example in Bazilevs et al.(2007) [54], Shakib and Hughes (1991) [20]), but when the steady-state is reached the subscale $\tilde{\boldsymbol{u}}$ that is obtained to solution of equation (4.17) satisfies $\tilde{\boldsymbol{u}} = \tau_1\tilde{P}(\boldsymbol{R}_u)$, so that the usual expression employed for stationary problems is recovered.

2. Suppose for example that the backward Euler scheme is used to integrate the equation (4.17). From the point of view of the algebraic solver, the factor $((1/\delta t) + (1/\tau_1))^{-1}$, instead of τ_1 is crucial for the conditioning of the system matrix. If τ_1 is used as stabilization factor, when $\delta t \to 0$(and thus the leading terms are those coming from the discretization of the time derivative) both the Galerkin and stabilizing terms could lead to matrix terms of the same order and the condition number of the matrix of the Galerkin method could be deteriorated.

3. It is clear that space discretization (understood as scale splitting) and time discretization commute, that is time discretization + stabilization (scale splitting) = stabilization (scale splitting) + time discretization.

4. Numerical experiments show that the temporal time integration is significantly improved:

   - oscillations originated by initial transients are eliminated; and
   - the numerical dissipation is minimized. For the numerical results that demonstrate this fact we refer to Codina et al. (2007) [42], Codina and Principe (2007) [12].

5. The numerical analysis shows optimal stability without any restriction between τ_1 and δt. Contrary to classical stabilized methods, anisotropic space-time discretizations are allowed (Bochev et al.2007 [36]). See Codina et al.2007 [42] for a stability analysis of the linearized Navier-Stokes equations and Badia and Codina 2009 [4] for a complete stability and convergence analysis for the Stokes problem.

4.4 Conservation of linear momentum and heat

In order to study the conservation properties of the scheme, we consider the extended problem which includes the boundary fluxes $B_{R,u}(\boldsymbol{v}_h)$ and $B_{R,\vartheta}(\psi_h)$ in the Navier Stokes and heat equations Hughes and Wells.2005 [25]. These fluxes may include contributions from the convective term when $\boldsymbol{a}$ is not divergence free, which may change according to the form used for this term (non-conservative, conservative or skew symmetric). This problem can be understood locally in a region R formed by an arbitrary set of elements (Hughes and Wells.2005 [25]), case in which boundary contributions come from the fluxes exchanged with the rest of the computational domain.

Another important remark is that the expression used for the convective term might not be the most convenient one. For divergence free velocity fields vanishing on the domain boundary, we have that:

$$\langle \boldsymbol{u}\cdot\nabla\boldsymbol{u},\boldsymbol{v}\rangle = -\langle \boldsymbol{u}\otimes\boldsymbol{u},\nabla\boldsymbol{v}\rangle = \frac{1}{2}\langle \boldsymbol{u}\cdot\nabla\boldsymbol{u},\boldsymbol{v}\rangle - \frac{1}{2}\langle \boldsymbol{u}\otimes\boldsymbol{u},\nabla\boldsymbol{v}\rangle$$

Any of these expressions can be used in the convective term of the approximate Navier-Stokes equations without altering the consistency. However, the discrete problem has different properties, as we will see. Thus, given vector field $\boldsymbol{a}$ we introduce:

$$c_u(\boldsymbol{a},\boldsymbol{u},\boldsymbol{v}) = \begin{cases} c_u^{nc}(\boldsymbol{a},\boldsymbol{u},\boldsymbol{v}) = \langle \boldsymbol{a}\cdot\nabla\boldsymbol{u},\boldsymbol{v}\rangle, & \text{Non conservative form} \\ c_u^{c}(\boldsymbol{a},\boldsymbol{u},\boldsymbol{v}) = -\langle \boldsymbol{a}\otimes\boldsymbol{u},\boldsymbol{v}\rangle, & \text{Conservative form} \\ c_u^{ss}(\boldsymbol{a},\boldsymbol{u},\boldsymbol{v}) = \frac{1}{2}\langle \boldsymbol{a}\cdot\nabla\boldsymbol{u},\boldsymbol{v}\rangle - \frac{1}{2}\langle \boldsymbol{a}\otimes\boldsymbol{u},\boldsymbol{v}\rangle, & \text{Skew-symmetric form} \end{cases}$$

Similarly, for the temperature equation we introduce:

$$c_\vartheta(\boldsymbol{a},\vartheta,\psi) = \begin{cases} c_\vartheta^{nc}(\boldsymbol{a},\vartheta,\psi) = \langle \boldsymbol{a}\cdot\nabla\vartheta,\psi\rangle, & \text{Non conservative form} \\ c_\vartheta^{c}(\boldsymbol{a},\vartheta,\psi) = -\langle \boldsymbol{a}\vartheta,\nabla\psi\rangle, & \text{Conservative form} \\ c_\vartheta^{ss}(\boldsymbol{a},\vartheta,\psi) = \frac{1}{2}\langle \boldsymbol{a}\cdot\nabla\vartheta,\psi\rangle - \langle \boldsymbol{a}\vartheta,\nabla\psi\rangle, & \text{Skew-symmetric form} \end{cases}$$

The terms "conservative"and "non-conservative"are classical in the CFD community. The term "skew-symmetric"refers to the fact that:

$$c_u^{ss}(\boldsymbol{a},\boldsymbol{u},\boldsymbol{u}) = 0, \quad c_\vartheta^{ss}(\boldsymbol{a},\vartheta,\vartheta) = 0$$

even if $\boldsymbol{a}$ is not divergence free.

Using the approximation $\tau_2 = 0$, defining $\boldsymbol{a} = \boldsymbol{u}_h + \tilde{\boldsymbol{u}}$ (which is solenoidal prior to the approximation of the subscales), introducing the possibilities for the convective term described and accounting for the boundary fluxes, problems (4.20-4.22) can be formulated like:

$$\begin{aligned}(\partial_t \boldsymbol{u}_h, \boldsymbol{v}_h) + (\boldsymbol{u}_h \cdot \nabla \boldsymbol{u}_h, \boldsymbol{v}_h) + \nu(\nabla \boldsymbol{u}_h, \nabla \boldsymbol{v}_h) - (p_h, \nabla \cdot \boldsymbol{v}_h) + \alpha(\boldsymbol{g}\vartheta_h, \boldsymbol{v}_h) \\ -\langle \tilde{\boldsymbol{u}}, \nu\Delta_h \boldsymbol{v}_h + \boldsymbol{u}_h \cdot \nabla \boldsymbol{v}_h\rangle = \langle \boldsymbol{f}, \boldsymbol{v}_h\rangle + \alpha(\boldsymbol{g}\vartheta_0, \boldsymbol{v}_h) + B_{R,u}(\boldsymbol{v}_h),\end{aligned} \tag{4.34}$$

$$(q_h, \nabla \cdot \boldsymbol{u}_h) - (\tilde{\boldsymbol{u}}, \nabla q_h) = 0, \tag{4.35}$$

$$\begin{aligned}(\partial_t \vartheta_h, \psi_h) + \langle \boldsymbol{u}_h \cdot \nabla \vartheta_h, \psi_h\rangle + \kappa(\nabla \vartheta_h, \nabla \psi_h) \\ -\langle \tilde{\vartheta}, \kappa\Delta_h \psi_h + \boldsymbol{u}_h \cdot \nabla \psi_h\rangle = \langle Q, \psi_h\rangle + B_{R,\vartheta}(\psi_h)\end{aligned} \tag{4.36}$$

As mentioned earlier, we may understand that this problem is posed in a region $R \subset \Omega$ formed by an arbitrary union of elements K of the finite element partition. When $R = \Omega$, $B_{\Omega,u}(\boldsymbol{v}_h) = 0$ and $B_{\Omega,\vartheta}(\psi_h) = 0$ with homogeneous boundary conditions. Otherwise, these boundary terms may depend on the way the convective term is written, but in any case they will be due to the action exerted by the fluid outside R on its boundary.

Let $\boldsymbol{e}_k$ be the vector of $\mathbb{R}$ with the k-th component equal to 1 and the rest equal to 0. Taking $\boldsymbol{v}_h = \boldsymbol{e}_k$ in Equation (4.34) it follows that:

$$\frac{d}{dt}\int_R \boldsymbol{u}_{h,k} + c_u(\boldsymbol{a};\boldsymbol{u}_h,\boldsymbol{e}_k) = \int_R [f_k + \alpha \boldsymbol{g}_k(\vartheta_0 - \vartheta_h)] + B_{R,u}(\boldsymbol{e}_k)$$

where $c_u(\boldsymbol{a};\boldsymbol{u}_h,\boldsymbol{e}_k)$ is the convective term and this equation can be understood as a conservation of linear momentum in a region R provided $c_u(\boldsymbol{a};\boldsymbol{u}_h,\boldsymbol{e}_k) = 0$ or has only contributions on ∂R. If the conservative form of the convective term is used it is obvious that $c_u^c(\boldsymbol{a};\boldsymbol{u}_h,\boldsymbol{e}_k) = -\langle \boldsymbol{a} \otimes \boldsymbol{u}_h, \nabla \boldsymbol{e}_k\rangle = 0$ so that the conservative form always conserves linear momentum. On the other hand, it is immediately checked that:

$$c_u^{nc}(\boldsymbol{a};\boldsymbol{u}_h,\boldsymbol{e}_k) = -\int_R u_{h,k}\nabla \cdot \boldsymbol{u}_h + \int_R \tilde{\boldsymbol{u}} \cdot \nabla u_{h,k} + \int_{\partial R} (\boldsymbol{n} \cdot \boldsymbol{u}_h) u_{h,k}$$

where $\boldsymbol{n}$ is the unit normal exterior to ∂R and the non-conservative form $c_u^{nc}(\boldsymbol{a};\boldsymbol{u}_h,\boldsymbol{e}_k) = \langle \boldsymbol{a} \cdot \nabla \boldsymbol{u}_h, \boldsymbol{e}_k\rangle$. From Equation (4.35), it follows that the first two terms in this equation are zero, provided we can take $q_h = u_{h,k}$. Thus, the nonconservative form conserves linear momentum if equal velocity-pressure interpolations are used. Note that this would not be possible using the Galerkin method. This fact was already noticed in (Hughes and Wells.2005 [25]).

From the expression of the skew-symmetric form of the convective term $c_u^{ss}(\boldsymbol{a};\boldsymbol{u},\boldsymbol{v}) = \frac{1}{2}\langle \boldsymbol{a} \cdot \nabla \boldsymbol{u}, \boldsymbol{v}\rangle - \frac{1}{2}\langle \boldsymbol{a} \otimes \boldsymbol{u}, \nabla \boldsymbol{v}\rangle$, it is clear that it has the same properties as the non-conservative form, since now:

$$c_u^{ss}(\boldsymbol{a};\boldsymbol{u}_h,\boldsymbol{e}_k) = -\frac{1}{2}\int_R u_{h,k}\nabla \cdot \boldsymbol{u}_h + \frac{1}{2}\int_R \tilde{\boldsymbol{u}} \cdot \nabla u_{h,k} + \int_{\partial R} (\boldsymbol{n} \cdot \boldsymbol{u}_h) u_{h,k}$$

A similar analysis can be undertaken for the heat equation. If $\psi_h = 1$ in Equation (4.36) it follows that:

$$\frac{d}{dt}\int_R \vartheta_h + c_\vartheta(\boldsymbol{a};\vartheta_h,1) = \int_R Q + B_{R,\vartheta}(1)$$

This equation can be understood as a conservation of heat in a region R provided $c_\vartheta(\boldsymbol{a};\vartheta_h,1) = 0$ or contributes only with terms defined on ∂R. Once again, if the conservative form of the convective term is used,$c^c_\vartheta(\boldsymbol{a};\vartheta_h,1) = -\langle \boldsymbol{a}\vartheta, \nabla 1\rangle = 0$, so that the conservative form always conserves heat. On the other hand:

$$c^{nc}_\vartheta(\boldsymbol{a};\vartheta_h,1) = -\int_R \vartheta_h \nabla\cdot\boldsymbol{u}_h + \int_R \tilde{\boldsymbol{u}}\cdot\nabla\vartheta_h + \int_{\partial R}(\boldsymbol{n}\cdot\boldsymbol{u}_h)\vartheta_h$$

From Equation (4.35), it follows that the first two terms in this equation are zero, provided we can take $q_h = \vartheta_h$. Thus, the non-conservative form conserves heat if equal temperature pressure interpolations are used. As for the Navier-Stokes equations, the same conclusion applies to the skew-symmetric form of the convective term in the heat equation.

4.5 Modeling turbulence

Let us conclude this chapter with some speculative comments on the contribution of the term $-\langle\tilde{\boldsymbol{u}},\tilde{\boldsymbol{u}}\cdot\nabla\boldsymbol{v}_h\rangle$. In the standard large eddy simulation (LES) approach to solve turbulent flows(see e.g.,S. Pope2000 [37]) an equation is obtained for the large, filtered scales of the flow, which we will denote with an overbar. This equation includes an extra term when compared with the incompressible Navier-Stokes equations(4.1-4.2) the divergence of the so-called *residual stress tensor* or sub-grid scale tensor $\boldsymbol{R} := \overline{\boldsymbol{u}\otimes\boldsymbol{u}} - \bar{\boldsymbol{u}}\otimes\bar{\boldsymbol{u}}$. Tensor $\boldsymbol{R}$ has to be modelled in terms of $\bar{\boldsymbol{u}}$ to obtain a self-contained equation, a problem known as the closure problem and once this is done, the resulting LES equation can be solved numerically.

The residual stress tensor, $\boldsymbol{R}$ is often decomposed into the so-called Reynolds, Cross and Leonard stresses to keep the Galilean invariance of the original Navier-Stokes equation in the LES equation. This invariance is automatically inherited by the formulation presented in this work and we observe that analogous terms to the various stress types are recovered in a "natural"way from our pure numerical approach (this was also the case in Hughes et al.2000 [50]). Let us have a look at this point. We first consider the last four terms in the material derivative:

$$\begin{aligned}\frac{D}{Dt}\boldsymbol{u} &= \frac{D}{Dt}(\boldsymbol{u}_h+\tilde{\boldsymbol{u}})\\ &= \partial_t\boldsymbol{u}_h + \partial_t\tilde{\boldsymbol{u}} + \tilde{\boldsymbol{u}}\cdot\nabla\boldsymbol{u}_h + \boldsymbol{u}_h\cdot\nabla\boldsymbol{u}_h + \tilde{\boldsymbol{u}}\cdot\nabla\tilde{\boldsymbol{u}} + \boldsymbol{u}_h\cdot\nabla\tilde{\boldsymbol{u}}\end{aligned}$$

as they appear in the variational equation (4.20). The term $-\langle\tilde{\boldsymbol{u}},\tilde{\boldsymbol{u}}\cdot\nabla\boldsymbol{v}_h\rangle$ can be rewritten as:

$$-\langle\tilde{\boldsymbol{u}},\tilde{\boldsymbol{u}}\cdot\nabla\boldsymbol{v}_h\rangle = -\langle\tilde{\boldsymbol{u}}\otimes\tilde{\boldsymbol{u}},\nabla\boldsymbol{v}_h\rangle$$

and can be identified with the Reynolds stress. The addition of the other three terms becomes, after integration by parts,

$$\langle\boldsymbol{u}_h\cdot\nabla\boldsymbol{u}_h,\boldsymbol{v}_h\rangle - \langle\tilde{\boldsymbol{u}},\boldsymbol{u}_h\cdot\nabla\boldsymbol{v}_h\rangle + \langle\tilde{\boldsymbol{u}}\cdot\nabla\boldsymbol{u}_h,\boldsymbol{v}_h\rangle = -\langle\boldsymbol{u}_h\otimes\boldsymbol{u}_h,\nabla\boldsymbol{v}_h\rangle - \langle\boldsymbol{u}_h\otimes\tilde{\boldsymbol{u}}+\tilde{\boldsymbol{u}}\otimes\boldsymbol{u}_h,\nabla\boldsymbol{v}_h\rangle$$

and we can identify the second term on the right hand side with the cross stress. If we now pay attention to the convective term of the residual $\boldsymbol{R}_u$ in the subscale equation (4.17) and take, for

simplicity, $\tilde{P} = I$, we observe that

$$\langle (\boldsymbol{u}_h + \tilde{\boldsymbol{u}}) \cdot \nabla \boldsymbol{u}_h, \tilde{\boldsymbol{v}} \rangle = -(\boldsymbol{u}_h \otimes \boldsymbol{u}_h, \nabla \tilde{\boldsymbol{v}}) - (\boldsymbol{u}_h \otimes \tilde{\boldsymbol{u}}, \nabla \tilde{\boldsymbol{v}})$$

and the first term on the right hand side can be identified with the Leonard stress. Hence, we can effectively conclude that the modifications introduced by the presence of the divergence of $\boldsymbol{R}$ in the LES equations are somehow automatically included in our subgrid scale stabilized finite element approach. Therefore, we may expect that, in some sense, modeling $\tilde{\boldsymbol{u}}$ implies to model the subgrid scale tensor. The question is how good this model will be. The numerical models proposed here yield two possibilities depending on the projection chosen, but others can be devised.

How good our formulation will work as a turbulent model will mainly depend on the validity of the approximation made to derive the evolution equation for the subscales (4.17), being the ASGS or the OSS methods two available possibilities. In order to check this performance, benchmark problems for turbulent flows should be used. A widely used benchmark problem is the decay of isotropic turbulence. Our model should be able to reproduce the Kolmogorov energy cascade in the wavenumber Fourier space that displays an inertial range, where $E(k) \sim C_K \varepsilon^{2/3} k^{-5/3}$ (ε being the energy dissipation rate, k the wavenumber modulus, C_K the Kolmogorov constant in energy space and E the kinetic energy). The model should be also able to capture the appropriate decay in time of energy, entropy and other related statistical variables. Other more intricate questions such as if the model allows for backscatter or if the dimension of the global attractor is properly reproduced could be also addressed. We remind that the heuristic estimate for this dimension is $N \sim (L/\lambda_K)^3 \sim Re^{9/4}$ (where λ_K is the Kolmogorov length scale) and that the closest estimate analytically proved is (roughly) $(L/\lambda_K)^{4.8}$(see Gibbon.et.al.1997 [22]). Finally, we should mention that in an attempt to find a more mathematical foundation for the LES approach to turbulence, the concept of suitable approximations to the Navier-Stokes equations has been introduced in J. Guermond et.al.2004 [27].

Related to the way turbulence is modelled, the numerical formulation proposed has an inherent turbulent Prandtl number. In other words, it is not necessary to specify which is the amount of turbulent thermal dissipation, but emanates directly from the formulation. This issue has been discussed in Codina.et.al.2010 [41].

Chapter 5

Numerical example of thermally coupled incompressible flows

In this chapter we present the results of two numerical tests involving two-dimensional thermally coupled flows. In both cases we have used Quasi static sub-scales with stabilization of $\tilde{P} = I$ referred to as Algebraic sub-grid scale method(ASGS) in (4.20-4.22), which corresponds to the most classical stabilized finite element methods, and $\tilde{P} = P_h^{\perp}$ referred to as Orthogonal sub-scale(QSS) stabilization in (4.23-4.25), which was proposed by Codina2002 [13].

In both numerical examples Quasi-static sub-scales used with ASGS and OSS stabilization method using three types of shock capturing techniques Isotropic diffusion(ID) residual based, Anisotropic crosswind diffusion(CD) residual based and Orthogonal projection gradient based diffusion (OPGB) for thermal equation discussed in chapter 3 for simple convection-diffusion equation. For the first numerical test coarse mesh will be considered to reproduce the exact results of finer mesh using shock capturing techniques. In these numerical examples mainly the comparison of the different combination of stabilization and shock capturing techniques will be discussed.

5.1 Flow in a differentially heated cavity with aspect ratio 8:1

As a first example of application of the formulation presented, we have modelled the flow in a differentially heated cavity with aspect ratio 8 by 1. The data of the problem can be found in Christon et.al.2002 [34]. Figure (5.1) shows the differential heated cavity of aspect ratio 8 where flow will be circulated due to buoyancy of the fluid because of the Boussinesq condition implied in this problem. This differential heated cavity is 1 unit wide and 8 units of height, insulated on horizontal walls and constant temperature on vertical walls, see figure (5.1). The interest of this problem is how the shock capturing techniques works with stabilization methods ASGS and OSS for the thermal equation and to compare the results using a finer mesh.

Three types of shock capturing techniques used for the elimination of local oscillations with the stabilized method ASGS and OSS will be tested. These three types of shock capturing or discontinuity capturing techniques are Isotropic diffusion(ID), Cross wind anisotropic diffusion (CD) residual based and Orthogonal projection gradient based (OPGB) shock capturing. For the first two shock capturing techniques ASGS stabilization used and OPGB shock capturing is used along with the OSS stabilization method for the temperature equation.

The Rayleigh number used here is $Ra = 3.45 \times 10^5$ where it is known that a Hopf bifurcation has occurred and the flow is oscillatory. The purpose of this numerical test is to compare the results using coarse mesh with shock capturing techniques with the results obtained by using a finer mesh. Moreover we tried to find out which combination of shock capturing techniques is better along with stabilization based on ASGS and OSS.

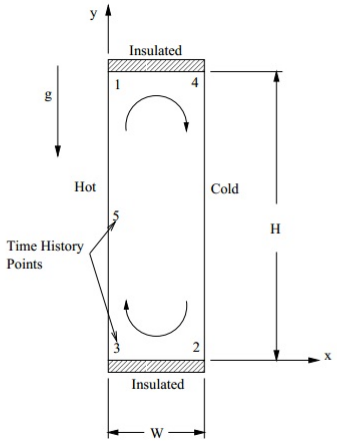

Fig. 5.1: Differential heated enclosure with 8:1 aspect ratio, insulated horizontal walls and constant temperature vertical walls.

The following results have been obtained using coarse mesh of 1510 nodal points and 2792 triangular linear elements. A second order Adams Bashforth time integration scheme and Picard linearization has been used for the Navier-Stokes equation, whereas the subscales have been integrated using a backward Euler scheme. The time step size used is 0.1. The value of the shock capturing parameter is used 0.7 because of using triangular linear elements (see Codina1993 [8]).

Comparing the results shown in Fig.(5.2) it is seen that using ASGS+ID and ASGS+CD combi-

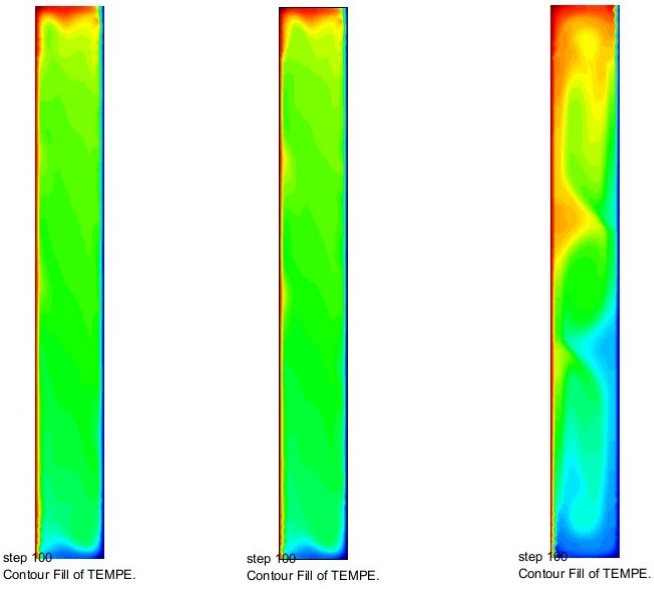

Fig. 5.2: Temperature contours from left ASGS+ID, middle ASGS+CD and right OSS+OPGB Rayleigh numbers: 3.45×10^5.

nations exhibit similar resolution, worse than using the combination OSS+OPGB. Here using the

Orthogonal projection gradient based(OPGB) shock capturing the solution provides similar result to those of using finer mesh(from figure 5.3). Here both ID and CD shock capturing techniques with ASGS stabilization parameter cannot resolve the similar solution of using finer mesh, see figure (5.3), where Hopf-bifurcation occurs due to using Rayleigh No, $Ra = 3.45 \times 10^5$. For finer mesh the following results have been obtained on a mesh of 10,721 nodal points and 10,500 bilinear quadrilateral elements. The OSS+OPGB method exhibits Hopf bifurcation and oscillatory results

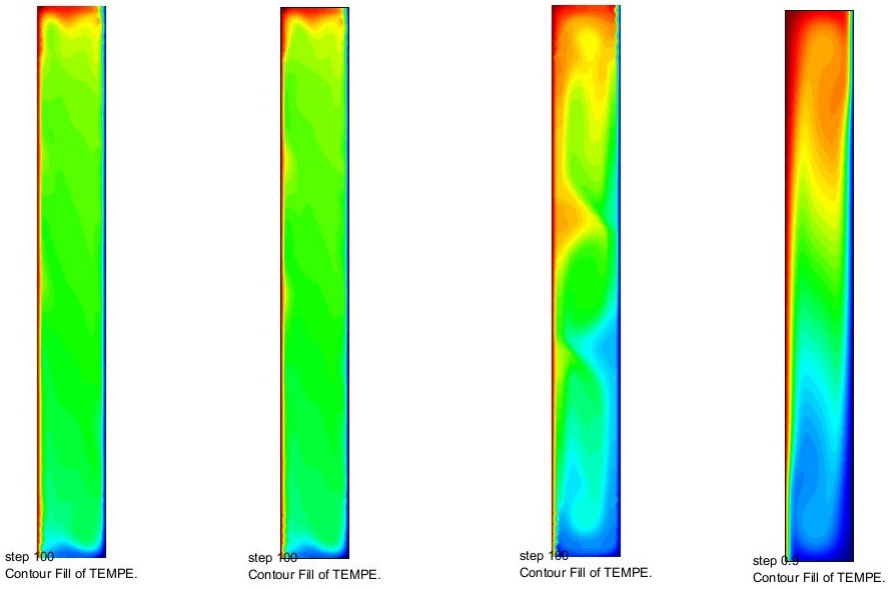

Fig. 5.3: Comparison of temperature contours from first ASGS+ID, second ASGS+CD and third OSS+OPGB, fourth using finer mesh without shock capturing Rayleigh numbers: 3.45×10^5.

which are similar to those we found using the fine mesh. Using the combination Orthogonal sub-grid scale stabilization with Orthogonal projection gradient based(OPGB) shock capturing resolves bifurcated behaviour and transition from steady to time-periodic behaviour, what usually found when using finer meshes.

5.2 2D Numerical modeling of hot fluid injection in a storage tank

For this numerical test we took an industrial problem in 2D for doing simple analysis to check how the shock capturing methods work to eliminate local instabilities. The main objective of this work is to capture all the phenomena generally present in a day of full operation of specially hot fluid dosing in the storage tank at a drinking water treatment plant. In this section we show the numerical results of simple used hot fluid injection in a water tank. There is an inflow in the upper surface and outflow at lower right surface. For this example simple rectangular domain considered of width $W = 13$ unit and height $H = 3.367$ unit with a pipe diameter of $D = 0.15$ unit at the inflow and outflow. The thermal conductivity is taken $k = 10^{-8}$, the viscosity as 1 and the Rayleigh number$= 4.55 \times 10^5$.

5.2.1 Boundary Conditions

The boundary conditions are simple and consists of no slip walls, insulated(zero heat flux) horizontal and vertical walls except at inflow in the upper wall, the temperature value is fixed to

	Left wall $x = 0$	Right wall $x = W$	Bottom Wall $y = 0$
Velocity BC's	$u_x = u_y = 0$	$u_x = u_y = 0$	$u_x = u_y = 0$
Temperature BC's	$\frac{\partial \vartheta}{\partial x} = 0$	$\frac{\partial \vartheta}{\partial x} = 0$	$\frac{\partial \vartheta}{\partial y} = 0$

	Top wall $y = H$	inflow at top	Outflow at the bottom right
Velocity BC's	$u_x = u_y = 0$	$u_x = 0.401462464$, $u_y = -0.401462464$	no velocity BC's
Temperature BC's	$\frac{\partial \vartheta}{\partial y} = 0$	$\vartheta = 0.00035$	free

Tab. 5.1: Velocity and temperature boundary conditions for Navier-stokes and Temperature equations.

0.00035 and at the outflow the heat flux is zero. The no slip and no penetration conditions are prescribed as $u_x = u_y = 0$ on all walls except at the inflow, where the constant velocity condition is $(u_x, u_y) = (0.401462464, -0.401462464)$. At the outflow the traction is zero(see figure 5.4).

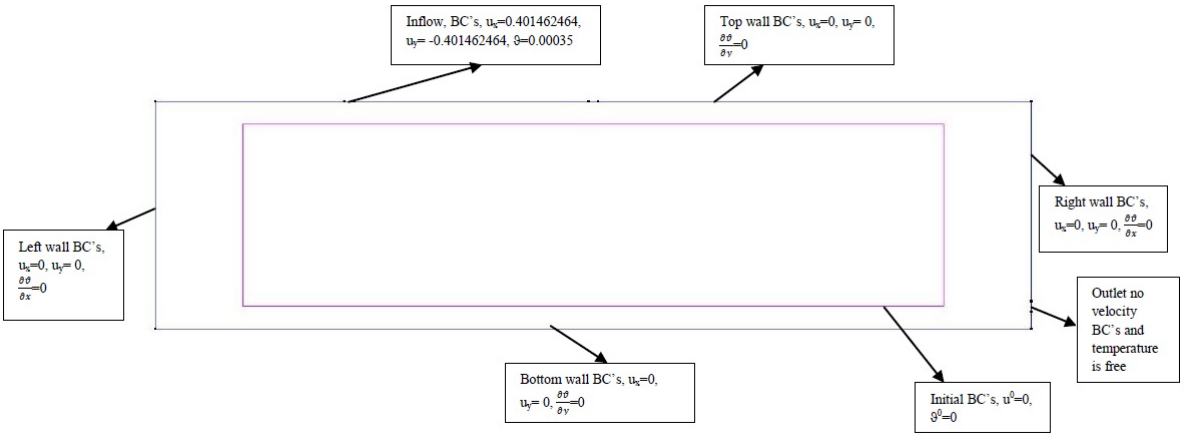

Fig. 5.4: 2D tank initial and boundary conditions.

5.2.2 Initial boundary condition

In this section, we describe one set of initial conditions for velocity and temperature (see figure 5.4) that may be used for a transient simulation. Here the fluid is isothermal and initially at rest:

$$\boldsymbol{u}(\boldsymbol{x}, \boldsymbol{y}, 0) = 0,$$

and

$$\vartheta(\boldsymbol{x}, 0) = 0$$

5.2.3 2D mesh of the tank problem

Here this is the 2D geometry of hot fluid injection in a water tank. We used a mesh of linear triangular elements of 2,137 nodal points with 3,948 elements. For better numerical results of hot fluid injection we used finer mesh at the inflow and outflow. Here we actually used one inflow condition at the upper left of the top wall while the upper right inflow is not considered here. The 2D mesh of the rectangular water tank is in the following figure (5.5).

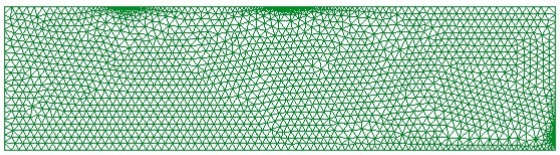

Fig. 5.5: 2d mesh of a rectangular water tank.

Temperature Equation	
Stabilization method	Shock capturing techniques
Algebraic sub-grid scale(ASGS)	Isotropic Diffusion(ID)
Algebraic sub-grid scale(ASGS)	Crosswind Diffusion (CD)
Orthogonal sub-scale (OSS)	Orthogonal projection gradient based (OPGB)

Tab. 5.2: Different combination of stabilization method and shock capturing techniques.

5.2.4 Numerical results

For this 2D tank problem hot fluid is injected from the top wall with the certain constant inflow velocity prescribed earlier and we mainly forecast here how the different combination of stabilization and shock capturing techniques work in this 2D problem. The different combination of stabilization and shock capturing techniques for the temperature equation and Navier Stokes equation used here are indicated in table (5.2). For the Navier stokes equation, Orthogonal sub-scale stabilization is used without any shock capturing parameter.

One more point that we can check if mass conservation is preserved at the inflow and outflow of the tank if we assume that the mass of fluid inside the tank is constant. In the continuous problem as the mass is the conserved quantity in this case, we can infer that the mass that goes into the domain is exactly equal to the mass that comes out, which is the intuitive idea of mass conservation. In figure (5.6) we can see the flow problem described before. Fluid enters the tank from the top wall at the left side and leaves the domain at the bottom-right side of the wall. Here inlet and outlet are both the same size. The colours represent the velocity magnitude. For the temperature using the three

Fig. 5.6: Tank flow - Velocity Contours.

combinations of stabilization and shock capturing method of table(5.2) the results we found for this 2D water tank problem are shown in figure (5.7).

From figure (5.7) of temperature contours it can be seen that with the combination of ASGS+ID and ASGS+CD similar kind of results are obtained with instabilities around the propagation of

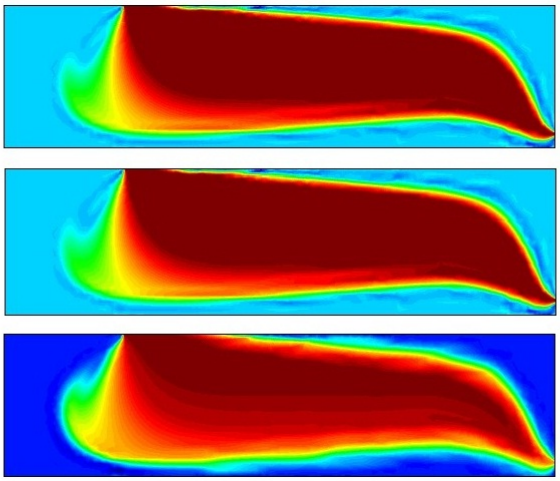

Fig. 5.7: Temperature contour from top ASGS+ID, middle ASGS+CD and bottom OSS+OPGB with Rayleigh numbers: 4.55×10^5.

the temperature contour from the inflow to the outflow. These methods cannot eliminate the local oscillation and instabilities while hot fluid is flowing from inflow(hot region) to outflow (colder region).

If we come to the case of OSS+OPGB combination of stabilization and shock capturing technique it provides better solutions, eliminating local oscillations while injection of hot fluid from inflow of upper wall to the outflow of lower right. This combination resolutes the exact highest and lowest temperature of this numerical test what we considered (initial inflow temperature equal to 0.00035 and outflow temperature equal to 0).

Comparing these three combination of stabilization and shock capturing techniques OSS+OPGB provides better numerical solution than ASGS+ID and ASGS+CD combinations, smoothing the outer contours of the temperature propagation profile and eliminating local instabilities and oscillations around sharp gradients.

Chapter 6

Industrial application of thermally coupled incompressible flow

In this chapter we extend our numerical application of the 2D hot fluid injection of a water tank problem to 3D. This example is a drinking-water storage tank used in Barcelona city. In fact, the modeling of the temperature is the same problem as the propagation of a concentration, for example chlorine. Minimizing short-circuit and dead zones, to guarantee treatment process efficiency, are problems commonly encountered in the design and optimization of water storage tanks. These tanks are the final phase of all common drinking water treatment plants; the process includes the mixing and contact tanks, the reaction and phase separation, storage and distribution (see H.Wang et.al.1998 [52]). Chlorine contact tank is the last treatment phase of the plant, and finally the treated water is stored in large tanks. Function of water storage tanks are twofold: equalize demand fluctuations (pumping requirements, operating pressures), and to provide storage for fire fighting and emergencies (see Rossman.et.al.1995 [31]). There are generally the storage tanks, where the mix of freshly inflow with the content of the tank is preferred and regulated. Water quality in storage tanks was not considered in early time for the design, but nowadays is a important objective to satisfy water regulations, that is why presence of total mix in the tank keep the bulk water quality.

Chlorine in present is the most common disinfectant used in drinking water treatment plants (other disinfectants used are ozone Z.Du-Quang.et.al.1999 [56],Kim.et.al.2010 [15] and ultraviolet Lyn.et.al.2005 [32], and in waste water treatment plant it is being used perioxyacetic acid as an alternative Santoro.et.al.2005 [16] substance). Computational modeling nowadays are widely used in studies of water treatment plants, for instance in chlorine contact tanks, setting tank and clarification basins; distribution system; bacterial inactivation; storage tanks and chlorine concentration decay see Greene.et.al.2006 [19]. The main consequence of chlorine decay (because its reactions with species) is that for long residence time of fluid particles inside tanks the amount of chlorine diminish (in fact exponentially), and poor concentration of disinfectant stimulates the bacterial regrowth. As the general normative required that minimum levels of chlorine must be maintained in the entry to the distribution system EPA [1] often is necessary a second re-chlorination in storage tanks H.Yeong2001 [55].

Modeling performance of real drinking water storage tanks consists of two stages, on the one hand it is necessary to simulate the hydrodynamic behaviour inside the tank according to inlet outlet configuration and pumping requirements. Some authors have mentioned the need of considering the variable water level in response to variable inlet-outlet flow, that is the flows are never steady H.Yeong2001 [55]. This numerical simulation is about chlorine injection in a storage tank taken from Codina.et.al.2010 [40]. We consider constant chlorine injection inside the water tank to make the numerical analysis simplified and also the flow at the outflow steady. Here mass conservation will

be preserved so that chlorine injection inflow will be equal to the outflow of the storage tank. Our main focus in this industrial based numerical simulation on chlorine injection jet rather than water flow inside the tank.

6.1 Geometry and dimension of the water storage tank

All design drawings of the water tank was provided by CETaqua. The case considered is Vallensana test case described in Codina.et.al.2010 [40]. The dimensions of the tank are shown in figure (6.1), where the hole diameter of the inflow and outflow are 0.15 and the length is 13 and height is 3.367, just similar to the previous 2D storage water tank problem.

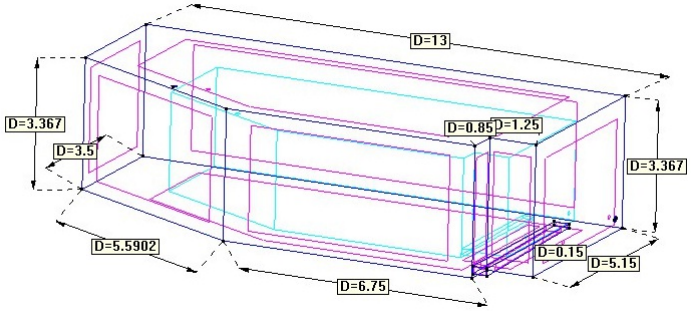

Fig. 6.1: Storage water tank dimension of vallensana test case.

Here there are two holes at the outflow and one hole at the inflow of the chlorine injection jet.

6.2 Boundary conditions

The boundary condition is just similar to the 2D case of the water tank problem that we have discussed in the previous chapter. Here the inflow chlorine jet boundary condition is not time dependent, what was considered in Vallensana test case reported in Codina.et.al.2010 [40]. We just use simple constant inflow boundary condition considered for chlorine jet $u_z = -0.56$ and at the two outer pipes the outflow velocity boundary conditions are fixed to zero traction. In all walls velocity boundary conditions were fixed to $u_x = u_y = u_z = 0$ except at the inflow hole. For the case of chlorine concentration, analogous to temperature boundary condition, at the inflow it was fixed to 0.00035 while at the two outflow temperatures were left free(see table 6.1).

	Left wall $x = 0$	Right wall $x = W$	Bottom Wall $y = 0$
Velocity BC's	$u_x = u_y = u_z = 0$	$u_x = u_y = u_z = 0$, except at the outflow	$u_x = u_y = u_z = 0$
Temperature BC's	$\frac{\partial \vartheta}{\partial x} = 0$	$\frac{\partial \vartheta}{\partial x} = 0$	$\frac{\partial \vartheta}{\partial y} = 0$

	Top wall $y = H$	inflow at top	Two outflow at the bottom right wall
Velocity BC's	$u_x = u_y = u_z = 0$	$u_z = -0.56$	no velocity BC's
Temperature BC's	$\frac{\partial \vartheta}{\partial y} = 0$	$\vartheta = 0.00035$	free

Tab. 6.1: Velocity and temperature boundary conditions.

6.3 Initial condition

In this section, we describe one set of initial conditions for velocity and temperature field that may be used for a transient simulation. Here the fluid is isothermal and initially at rest:

$$\boldsymbol{u}(\boldsymbol{x}, \boldsymbol{y}, \boldsymbol{z}, 0) = 0,$$

and

$$\theta(\boldsymbol{x}, \boldsymbol{y}, \boldsymbol{z}, 0) = 0$$

6.4 3D mesh of the storage tank

Here for this 3D geometry of the chlorine injection in a water change tank we used linear triangular elements of 28,633 nodal points with 124,789 elements which, is not so much finer mesh for this 3D geometry. For better numerical results of chlorine injection we used a finer mesh at the inflow and two outflow channels. The 3D mesh of the water tank is shown in figure (6.2).

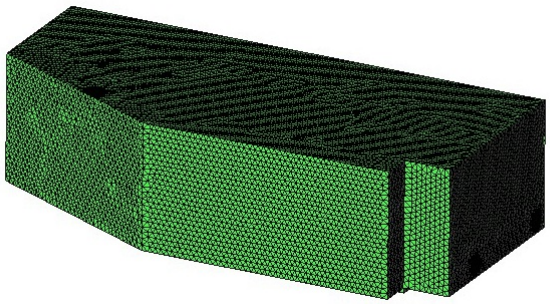

Fig. 6.2: 3d mesh of a storage water tank.

6.5 Numerical results

The main focus of this industrial water storage tank test is to do numerical analysis of the temperature profile of the injection jet inside the tank which can be understood as chlorine concentration. Here we used different combination of stabilization formulations and shock capturing methods to compare which method works better with the turbulent flow problem. The different combination of stabilization method and shock capturing techniques used for the temperature equation are given in table (6.2). For incompressible Navier-Stokes equations only Algebraic sub-grid scale(ASGS) stabilization has been used, with these three different combination of stabilization and shock capturing techniques for the temperature equation.

The Reynolds number used here is 168, where density is $\rho = 1$, velocity at the inlet $u = 0.56$, characteristic length (diameter of the pipe) $D = 0.15$, dynamic viscosity considered here $\mu = 0.5 \times 10^{-3}$. The Rayleigh number used here is 1.538×10^{6} with thermal conductivity $k = 1 \times 10^{-3}$, which is a turbulent case of convective flow. For this reason we used LES Smagorinsky turbulence model with the parameter $C_s = 0.1$. This problem is highly non-linear as because of the convective term. Picards method used here for linearization of Navier-Stokes convective term, and Generalized minimal residual method(GMRES) used as an algebraic solver. Here our main focus is to check

Temperature Equation	
Stabilization method	Shock capturing techniques
Algebraic sub-grid scale(ASGS)	Isotropic Diffusion(ID)
Algebraic sub-grid scale(ASGS)	Crosswind Diffusion (CD)
Orthogonal sub-scale (OSS)	Orthogonal projection gradient based (OPGB)

Tab. 6.2: Different combination of stabilization methods and shock capturing techniques used for this numerical example.

the performance of different stabilization methods and shock capturing techniques used for the temperature equation and how they avoid local oscillations.
Figure (6.3) shows the results obtained with different combination of stabilization and shock capturing methods employed for temperature profile after 1000 time steps at the inflow of the tank. It shows different numerical results for these three different cases. Comparing the Algebraic subscale using isotropic diffusion(ID) and anisotropic crosswind diffusion(CD) it shows oscillations during the propagation of temperature inside the tank. ASGS+ID combination shows more oscillations than ASGS+CD combination of stabilization and shock capturing methods, during the injection of the chlorine jet inside the tank.

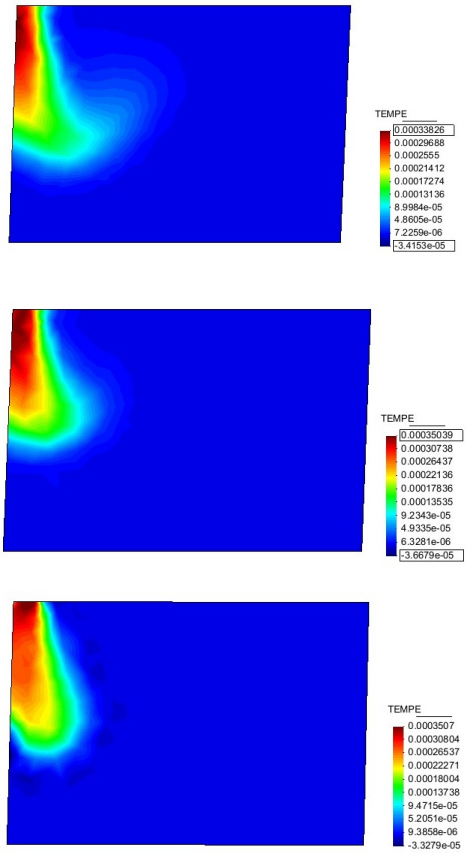

Fig. 6.3: Cross section of the tank of temperature contour at inflow of chlorine injection using different combination of stabilization and shock capturing techniques(From top ASGS+ID, middle ASGS+CD, bottom OSS+OPGB).

If we compare Orthogonal subscale(OSS) with Orthogonal projection gradient based(OPGB) shock

capturing with other two combinations(ASGS+ID and ASGS+CD) it can be concluded from figure (6.3) OSS+OPGB combination exhibits better results with less local oscillation during temperature propagation from the inflow into the water tank and spurious oscillations damped out by this combination of stabilization and shock capturing method. Moreover heat is transferring smoothly which is clearly visible from the temperature profile figure (6.3). It resolves the maximum temperature $\vartheta_{\text{max}} = 0.00035$ at inflow and minimum temperature $\vartheta_{\text{min}} = 0$ at the outflow exactly, without oscillations.

In figure (6.4) the velocity cut at the inflow of the tank has been shown for the three different combinations of stabilization and shock capturing methods.

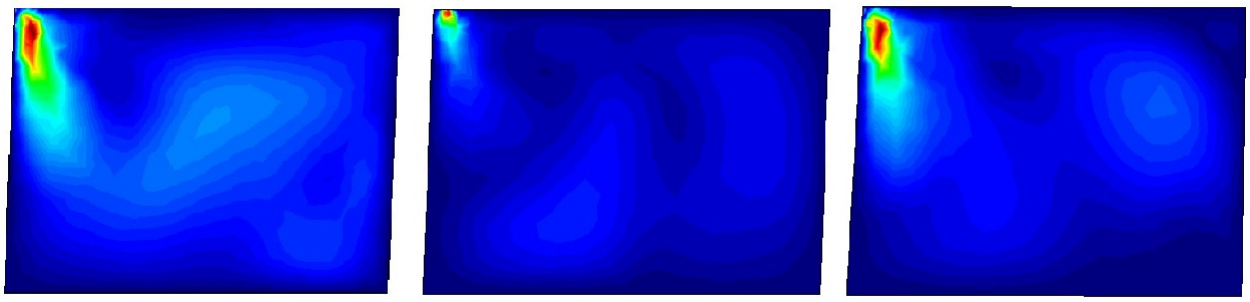

Fig. 6.4: Comparison of sectional view of velocity contour at the inflow of the tank ASGS+ID left, ASGS+CD middle and OSS+OPGB right.

The particle paths of velocity vectors are shown in figure (6.5) where they are all same for the three different cases.

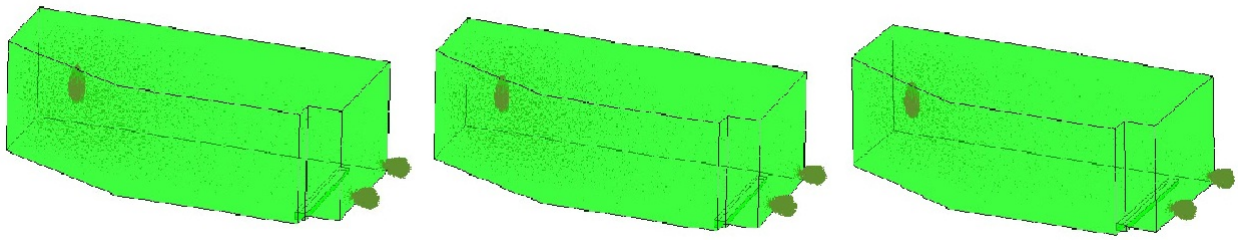

Fig. 6.5: Particle paths inside the tank for the three cases of ASGS+ID left, ASGS+CD middle and OSS+OPGB right.

In figure (6.6) pressure contours, in figure (6.7) velocity vector paths at the inlet of the tank and in figure (6.8) velocity streamlines inside the tank have been shown for three different cases of stabilization and shock capturing methods: ASGS+ID, ASGS+CD and OSS+OPGB.

Fig. 6.6: Comparison of cross section of pressure contour for the three cases of ASGS+ID left, ASGS+CD middle and OSS+OPGB right.

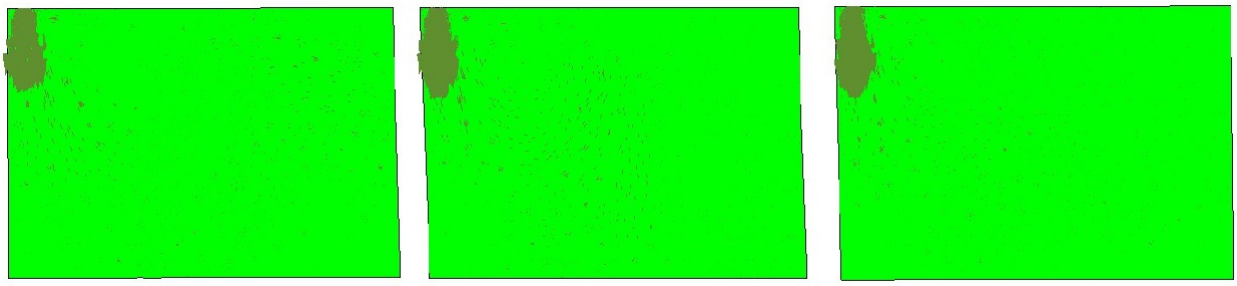

Fig. 6.7: Cross sectional view of velocity vectors at the inlet of the tank for three different cases.

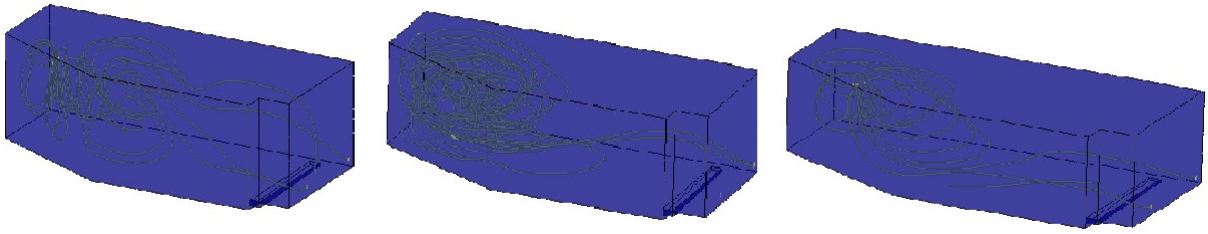

Fig. 6.8: Velocity streamlines inside the tank.

Chapter 7

Conclusion

7.1 Summary

The purpose of this thesis is to give an overview of a finite element formulation for thermally coupled incompressible flows whose intention is to go beyond stabilized finite element methods and, more precisely, to allow to simulate turbulent flows. The space variation of the subscales is approximated in terms of the residual of the finite element unknowns in the classical way used in stabilized finite element methods, but now they are integrated in time. In particular, global momentum conservation and global heat conservation is obtained. Additionally, in the case of thermally coupled flows the coupling of velocity and temperature subscales is dealt with in a natural way. Even though most of the points have been treated succinctly, the main aspects of the method have been touched, namely:

- its derivation through a scale splitting in the variational multiscale context;
- stabilized formulation of Algebraic subgrid scale stabilization(ASGS) and Orthogonal subscale(OSS) stabilization;
- the possibility of considering dynamic subscales; and
- the choice of the space of subscales as orthogonal to the finite element space.
- Tracking of subscales along nonlinear process permits global conservation of momentum. It also opens the door to the possibility of modeling turbulence using LES.

The another main purpose of this thesis is to get the idea and to check performance tests of different combination of stabilization methods and shock capturing diffusion, how they work in the convection diffusion equation and thermally coupled incompressible flows using the Boussinesq approximation. The different combinations of stabilization and shock capturing diffusion discussed in this thesis, mainly used in temperature equation, are:

- Algebraic sub-grid scale(ASGS) stabilization with isotropic diffusion(ID) residual based shock capturing;
- Algebraic sub-grid scale(ASGS) stabilization with anisotropic crosswind diffusion(CD) residual based shock capturing; and
- Orthogonal sub-scale(OSS) stabilization with orthogonal projection gradient based(OPGB) shock capturing diffusion.

Using these three different combinations of stabilization and shock capturing diffusion it can be concluded that Orthogonal projection gradient based (OPGB) shock capturing diffusion performs

well along with the OSS stabilization in both convection diffusion equation and thermally coupled incompressible flows compared to the other two (ASGS+ID and ASGS+CD) combinations of stabilization and shock capturing techniques.

In the convection diffusion equation it exhibits smoother solution with less overdiffusive characteristics and provides better numerical solutions comparing to the other combinations of stabilization and shock capturing techniques.

In the numerical examples of thermally coupled incompressible flows it provides better numerical solution even using coarse meshes which similar results to those we can find using finer meshes eliminating local oscillation compared the other two shock capturing techniques. The ASGS with ID and CD combinations generate almost the same numerical results in this occasion, eliminating less local oscillations in the sharp boundary layers and being less accurate in general.

7.2 Further Improvement

Several research lines emerge from this thesis. The first important line is the modeling of the subgrid scales, what has been the main subject of this thesis as modeling velocity subscale is the main important part and modeling this means modeling the Reynolds stress tensor in LES. So it is important to show how good this model is. The numerical model proposed here yields two possibilities depending on the projection chosen(either identity or orthogonal to the finite element space), but others can be devised.

Another important aspect is that we only proposed here three different combinations of stabilization and shock capturing techniques to eliminate the local oscillations in the sharp layers. But there are several other combinations which can be tested for further research.

Bibliography

[1] Comprehensive surface water treatment rules quick reference guide: unfiltered systems, August 2004. EPA 816-F-04-001.

[2] D. Apsley. Turbulence modelling in cfd, 2004. CFD.

[3] S. Badia and R. Codina. Analysis of a stabilized finite element approximation of the transient convection-diffusion equation using an ale framework. *SIAM Journal on Numerical Analysis*, Volume 44(pp 2159-2197), 2006.

[4] S. Badia and R. Codina. On a multiscale approach to the transient stokes problem. transient subscales and anisotropic space-time discretization. *Applied Mathematics and Computation*, Volume 207:pp 415–433, 2009.

[5] Brian Bell. Turbulent flow case studies. Fluent Software Training UGM 2003.

[6] U. Navert C. Johnson and J. Pitkaranta. Finite element methods for linear hyperbolic equations. *Computer Methods in Applied Mechanics and Engineering*, Volume 45:285312, 1984.

[7] Jos Luis; Lisbona Francisco J. (Eds.) Clavero, Carmelo; Gracia. *Bail 2010 - Boundary and Interior Layers, Computational and Asymptotic Methods*, volume Volume 81, chapter Finite Element Approximation of the Convection-Diffusion Equation: Subgrid-Scale Spaces, Local Instabilities and Anisotropic Space-Time Discretizations. Springer, 2001.

[8] R. Codina. A discontinuity-capturing crosswind-dissipation for the finite element solution of the convection-diffusion equation. *Computer Methods in Applied Mechanics and Engineering*, Volume 110:pp 325–342, 1993.

[9] R. Codina. Stabilization of incompressibility and convection through orthogonal sub-scales in finite element methods. *Comput. Methods Appl. Mech. Engrg.*, Volume 190(pp 1579-1599), 2000.

[10] R. Codina. Stabilized finite element approximation of transient incompressible flows using orthogonal subscales. *Computer Methods in Applied Mechanics and Engineering*, Volume 191:pp 4295–4321, 2000.

[11] R. Codina. Analysis of a stabilized finite element approximation of the oseen equations using orthogonal subscales. *Applied Numerical Mathematics*, Volume 58:pp 264–283, 2008.

[12] R. Codina and J. Principe. Dynamic subscales in the finite element approximation of thermally coupled incompressible flows. *International Journal for Numerical Methods in Fluids*, Volume 54:pp 707–730, 2007.

[13] R. Codina and O. Zienkiewicz. Cbs versus gls stabilization of the incompressible navier-stokes equations and the role of the time step as stabilization parameter. *Communications in Numerical Methods in Engineering*, Volume 18:99112, 2002.

[14] Ramon Codina. A comparison of some finite element methods for solving the diffusion-convection-reaction equation. *Computer Methods in Applied Mechanics and Engineering*, Volume 156:pp 185–210, 12 April 1998.

[15] J.H. Kim D. Kim, D.I. Kim and T. Stoesser. Large eddy simulation of flow and tracer transport in multichamber ozone contactors. *Journal of Environmental Engineering*, Volume 136(1):pp 22–31, 2010.

[16] D.J. Greene B. Farouk C.N. Haas M. Notarnicola D. Santoro, T.A. Bartrand and L. Liberti. Use of cfd for wastewater disinfection process analysis: E.coli inactivation with peroxyacetic acid (paa). *International Journal of Chemical Reactor Engineering*, Volume 3(A46), 2005.

[17] Lars Davidson. Numerical methods for turbulent flow, 2005. Department of Applied Mecahnics, Chalmers University.

[18] Hallak P.H. Coutinho A.L.G.A. de Sampaio, P.A.B. and M.S. Pfeil. A stabilized finite element procedure for turbulent fluid-structure interaction using adaptive time-space refinement. *International Journal for Numerical Methods in Fluids*, Volume 44:pp 673–693, 2004.

[19] C.N. Hass D.J. Greene and B. Farouk. Computational fluid dynamics analysis of the effects of reactor configuration on desinfection efficiency. *Water Environment Research*, Volume 78:pp 909–919, 2006.

[20] and T.J.R Hughes F. Shakib. A new finite element formulation for computational fluid dynamics: Ix. fourier analysis of space-time galerkin/leastsquares algorithms. *Computer Methods in Applied Mechanics and Engineering*, Volume 87:pp 35–58, 1991.

[21] Professor William K. George. Lectures in turbulence for the 21st century. Professor of Turbulence, Chalmers University of Technology, Gothenburg, Sweden.

[22] J. Gibbon and E. Titi. Attractor dimension and small length scale estimates for the three dimensional navier-stokes equations. *Nonlinearity*, Volume 10:pp 109–119, 1997.

[23] J. Hoffman and C. Johnson. A new approach to computational turbulence modeling. *Computer Methods in Applied Mechanics and Engineering*, Volume 195(pp 2865-2880), 2006.

[24] T. J. R. Hughes and A. N. Brooks. A multidimensional upwind scheme with no crosswind diffusion. In editor In T. J. R. Hughes, editor, *FEM for convection dominated flows*, New York, 1979. ASME.

[25] T. J. R. Hughes and G. N. Wells. Conservation properties for the galerkin and stabilised forms of the advection-diffusion and incompressible navier-stokes equations. *Computer Methods in Applied Mechanics and Engineering*, Volume 194(9-11):pp 1141–1159, 2005.

[26] T.J.R Hughes. Multiscale phenomena: Greens function, the dirichlet-to-neumann formulation, sub-grid scale models, bubbles and the origins of stabilized formulations. *Computer Methods in Applied Mechanics and Engineering*, Volume 127:pp 387–401, 1995.

[27] J. Oden J. Guermond and S. Prudhomme. Mathematical perspectives on large eddy simulation models for turbulent flows. *Journal of Mathematical Fluid Mechanics*, 6:194248, 2004.

[28] R. Codina J. Principe and F. Henke. The dissipative structure of variational multiscale methods for incompressible ows. *Computer Methods in Applied Me- chanics and Engineering*, Volume 199:pp 791–801, 2010.

[29] E.S. Oran J.P. Boris, F.F. Grinstein and R.L. Kolbe. New insights into large-eddy simulation. *Fluid Dynamics Research*, Volume 10:pp 199–228, 1992.

[30] Dmitri Kuzmin. *A guide to numerical method for transport equation*. PhD thesis, Friedrich-Alexander-Universitat Erlangen Nurnberg, 2010.

[31] J.G. Uber L.A. Rossman and W.M. Grayman. Modeling disinfectant residuals in drinking-water storage tanks. *Journal of Environmental Engineering*, Volume 121(10):pp 752–755, 1995.

[32] D.A. Lyn and E.R. Blatchley. Numerical computational fluid dynamics-based models of ultraviolet disinfection channels. *Journal of Environmental Engineering*, Volume 131(6):pp 838–849, 2005.

[33] A. Uno T. Ishihara M. Yokokawa, K. Itakura and Y. Kaneda. 16.4-tflops direct numerical simulation of turbulence by a fourier spectral method on the earth simulator. 2002.

[34] P.M. Gresho M.A. Christon and S.B. Sutton. Computational predictability of natural convection flows in enclosures. *International Journal for Numerical Methods in Fluids*, Volume 40:pp 953–980, 2002.

[35] Steven Orszag. Analytical theories of turbulence. *Journal of Fluid Mechanics*, Volume 41:pp 363–386, 1970.

[36] M.D. P.B. Bochev, Gunzburger and R.B. Lehoucq. On stabilized finite element methods for the stokes problem in the small time-step limit. *International Journal for Numerical Methods in Fluids*, Volume 53:pp 573–597, 2007.

[37] S. Pope. *Turbulent Flows*. Cambridge University Press, 2000.

[38] J. Principe. *Subgrid scale stabilized finite elements for low speed flows*. PhD thesis, Universitat Politecnica de Catalunya, Barcelona, Spain, 2009.

[39] J. Principe R. Codina and J. Baiges. Subscales on the element boundaries in the variational two-scale finite element method. *Computer Methods in Applied Mechanics and Engineering*, Volume 198:pp 838–852, 2009.

[40] J. Principe Shu-Ren Hysing R. Codina, Christian Munoz. Cfd simulation of water treatment processes. Technical report, CIMNE, September 2010.

[41] Javier Principe R. Codina and Matias Avila. Finite element approximation of turbulent thermally coupled incompressible flows with numerical sub-grid scale modelling. *International Journal of Numerical Methods for Heat and Fluid Flow*, Volume 20(5):pp 492–516, February 2010.

[42] O. Guasch R. Codina, J. Principe and S. Badia. Time dependent subscales in the stabilized finite element approximation of incompressible flow problems. *Computer Methods in Applied Mechanics and Engineering*, Volume 196(21-24):pp 2413–2430, 1 April 2007.

[43] J.N. Reddy and D.K. Gartling. *The Finite Element Method in Heat Transfer And Fluid Dynamics*. CRC Press, London, 1994.

[44] Tony Saad. Turbulence modeling for beginners. UNIVERSITY OF TENNESSEE SPACE INSTITUTE.

[45] P. Sagaut. *Large Eddy Simulation for Incompressible Flows*. Springer, New York, 2001.

[46] S.B.Pope. *Turbulent Flows*. Cambridge University Press, 2000.

[47] S. Socolofsky. Lecture notes, Texas A and M University.

[48] Jurij SODJA. Turbulence models in cfd. Technical report, Faculty for mathematics and physics Department of physics, University of Ljubljana, March 2007.

[49] L. Mazzei T. J. R. Hughes, G. R. Feijoo and J. Quincy. The variational multiscale methoda paradigm for computational mechanics. *Computer Methods in Applied Mechanics and Engineering*, Volume 166(Issues 12):pp 13–24, 13 November 1998.

[50] L. Mazzei T.J.R Hughes and K.E. Jansen. Large-eddy simulation and the variational multiscale method. *Computing and Visualization in Science*, Volume 3:pp 47–59, 2000.

[51] Saarbrcken Volker John. On large eddy simulation and variational multiscale methods in the numerical simulation of turbulent incompressible flows. *APPLICATIONS OF MATHEMATICS*, Volume.4:pp. 321–353, 2006.

[52] H. Wang and R.A. Falconer. Numerical modeling of flow in chlorine disinfection tanks. *Journal of Hydraulic Engineering*, Volume 124(9):pp 918–931, 1998.

[53] D.C. Wilcox. *The Finite Element Method in Heat Transfer And Fluid Dynamics*. DCW Industries, Inc.

[54] J.A Cottrell T.J.R. Hughes A. Reali and G. Scovazzi Y. Bazilevs, V.M Calo. Variational multiscale residual-based turbulence modeling for large-eddy simulation of incompressible flows. *Computer Methods in Applied Mechanics and Engineering*, Volume 197:pp 173–201, 2007.

[55] H. Yeong. Modelling of service reservoirs. *Journal of Hydroinformatics*, Volume 3(3):pp 165–172, 2001.

[56] A. Line Z. Do-Quang, A. Cockx and M. Roustan. Computational fluid dynamics applied to water and wastewater treatment facility modeling. *Environmental Engineering and Policy*, Volume 1:pp 137147, 1999.